AGU PUBLICATIONS

Global Biogeochemical Cycles

RESEARCH ARTICLE
10.1002/2015GB005134

Key Points:
- Small particles are major contributors to particulate flux in summer
- Higher export efficiency associated with picoplankton and diazotrophs
- Global compilation of *b* terms linked to plankton dominance

Supporting Information:
- Readme
- Table S1

Correspondence to:
C. R. Benitez-Nelson,
cbnelson@geol.sc.edu

Citation:
Puigcorbé, V., C. R. Benitez-Nelson, P. Masqué, E. Verdeny, A. E. White, B. N. Popp, F. G. Prahl, and P. J. Lam (2015), Small phytoplankton drive high summertime carbon and nutrient export in the Gulf of California and Eastern Tropical North Pacific, *Global Biogeochem. Cycles*, *29*, 1309–1332, doi:10.1002/2015GB005134.

Received 3 MAR 2015
Accepted 29 JUL 2015
Accepted article online 2 AUG 2015
Published online 31 AUG 2015

Small phytoplankton drive high summertime carbon and nutrient export in the Gulf of California and Eastern Tropical North Pacific

Viena Puigcorbé[1], Claudia R. Benitez-Nelson[2], Pere Masqué[1,3,4], Elisabet Verdeny[1], Angelicque E. White[5], Brian N. Popp[6], Fredrick G. Prahl[5], and Phoebe J. Lam[7,8]

[1]Institut de Ciència i Tecnologia Ambientals and Departament de Física, Universitat Autònoma de Barcelona, Cerdanyola del Vallès, Barcelona, Spain, [2]Marine Science Program and Department of Earth & Ocean Sciences, University of South Carolina, Columbia, South Carolina, USA, [3]Oceans Institute and School of Physics, The University of Western Australia, Crawley, Western Australia, Australia, [4]School of Natural Sciences and Centre for Marine Ecosystems Research, Edith Cowan University, Joondalup, Western Australia, Australia, [5]College of Earth, Ocean and Atmospheric Sciences, Oregon State University, Corvallis, Oregon, USA, [6]Department of Geology and Geophysics, University of Hawaii, Honolulu, Hawaii, USA, [7]Department of Marine Chemistry and Geochemistry, Woods Hole Oceanographic Institution, Woods Hole, Massachusetts, USA, [8]Ocean Sciences Department, University of California Santa Cruz, Santa Cruz, California, USA

Abstract Summertime carbon, nitrogen, and biogenic silica export was examined using ^{234}Th:^{238}U disequilibria combined with free floating sediment traps and fine scale water column sampling with in situ pumps (ISP) within the Eastern Tropical North Pacific and the Gulf of California. Fine scale ISP sampling provides evidence that in this system, particulate carbon (PC) and particulate nitrogen (PN) concentrations were more rapidly attenuated relative to ^{234}Th activities in small particles compared to large particles, converging to 1–5 μmol dpm^{-1} by 100 m. Comparison of elemental particle composition, coupled with particle size distribution analysis, suggests that small particles are major contributors to particle flux. While absolute PC and PN export rates were dependent on the method used to obtain the element/^{234}Th ratio, regional trends were consistent across measurement techniques. The highest C fixation rates were associated with diatom-dominated surface waters. Yet, the highest export efficiencies occurred in picoplankton-dominated surface waters, where relative concentrations of diazotrophs were also elevated. Our results add to the increasing body of literature that picoplankton- and diazotroph-dominated food webs in subtropical regions can be characterized by enhanced export efficiencies relative to food webs dominated by larger phytoplankton, e.g., diatoms, in low productivity pico/nanoplankton-dominated regions, where small particles are major contributors to particle export. Findings from this region are compared globally and provide insights into the efficiency of downward particle transport of carbon and associated nutrients in a warmer ocean where picoplankton and diazotrophs may dominate. Therefore, we argue the necessity of collecting multiple particle sizes used to convert ^{234}Th fluxes into carbon or other elemental fluxes, including <50 μm, since they can play an important role in vertical fluxes, especially in oligotrophic environments. Our results further underscore the necessity of using multiple techniques to quantify particle flux given the uncertainties associated with each collection method.

1. Introduction

Oceanic particle cycling and export play major roles in the biogeochemical cycling of carbon and associated nutrients [*Honjo et al.*, 2008]. Yet understanding their magnitude and variability over temporal and spatial scales remains limited [*Burd et al.*, 2010]. Such knowledge is particularly needed as large-scale changes in climate are already influencing the marine system, as documented in ocean acidity, upper ocean circulation patterns, and the rate of particle export [*Feely et al.*, 2004; *Doney et al.*, 2012; *Taylor et al.*, 2012]. It has been hypothesized that future increases in global ocean temperatures will increase upper ocean stratification, thereby influencing a marine food web structure [*Richardson and Schoeman*, 2004; *Hays et al.*, 2005; *Doney*, 2006; *Beaugrand et al.*, 2008] that favors smaller phytoplankton [*Morán et al.*, 2010; *Taylor et al.*, 2012] and, likely, nitrogen-fixing organisms [*Karl et al.*, 2002; *Hutchins et al.*, 2007]. This shift in phytoplankton ecology may alter both particle flux and composition, with profound implications for marine biogeochemistry [*Bopp et al.*, 2005]. Increasing stratification has also been hypothesized to play a role in the significant areal and volumetric expansion of oxygen minimum zones [*Keeling et al.*, 2010], which further influences the

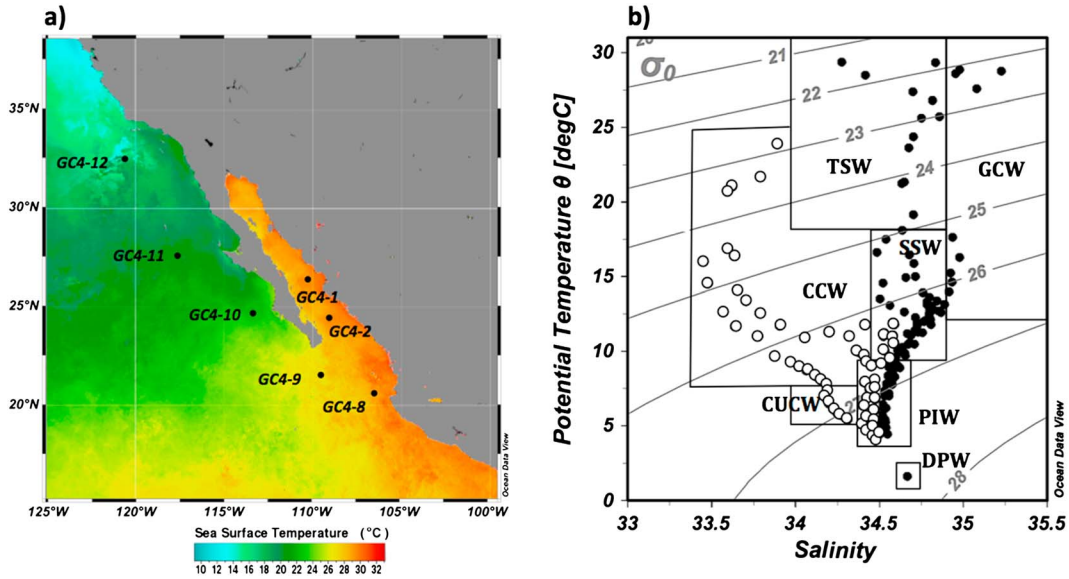

Figure 1. Hydrographic characteristics and location of the sampled stations. Figure 1a indicates the location of the stations along the Gulf of California and the eastern tropical North Pacific transect, overlain on the mean surface temperature for July 2008 derived from MODIS AQUA remote sensing data (http://oceancolor.gsfc.nasa.gov). Figure 1b corresponds to the T-S diagram of the upper 1000 m of the seven stations. At station GC4-8, sampling occurred down to 3000 m depth. Contour lines represent isopycnal surfaces (σ_θ). Open circles represent ETNP stations (GC4-10, GC4-11, and GC4-12). Filled circles represent Transition zone (GC4-8 and GC4-9) and GC (GC4-1 and GC4-2) stations. The rectangles represent different water masses: California Current Water (CCW), California Undercurrent Water (CUCW), Subtropical Subsurface Water (SSW), Pacific Intermediate Waters (PIW), Tropical Surface Waters (TSW), Gulf of California Waters (GCW), and Deep Pacific Water (DPW).

remineralization of particles as they sink through the water column [*DeVries and Deutsch*, 2014]. Thus, understanding the biogeochemistry of warm, stratified regions underlain by a strong oxygen minimum zone is of immediate and broad interest.

One such region is the Eastern Tropical North Pacific (ETNP), where more than 35% of global water column denitrification takes place [*Cline and Richards*, 1972; *Codispoti and Richards*, 1976]. The persistent oxygen minimum zone extends from the equator to 25°N and westward from the coast to 140°W [*Paulmier and Ruiz-Pino*, 2009]. ETNP suboxia, and thus denitrification, is maintained by a combination of remineralized particulate organic material [*Van Mooy et al.*, 2002] and both horizontal and vertical circulation/ventilation patterns [*Duteil and Oschlies*, 2011; *Gnanadesikan et al.*, 2012]. The Gulf of California (GC) is a subtropical semi-enclosed sea located along the southwest coast of North America (Figure 1). Suboxic and partly denitrified waters from the ETNP (i.e., N:P $<$ 16:1) enter into the central GC between 500 and 1000 m depth via the California Undercurrent, which also transports the denitrified waters to the north along the continental slope of North America [*Bray and Robles*, 1991; *Castro et al.*, 2001; *Liu and Kaplan*, 1989; *Roden*, 1958]. In winter, the GC is characterized by strong northwestern winds that induce upwelling. This physical oceanographic change results in high rates of nitrate-driven primary production [*White et al.*, 2007] and a biological community dominated by diatoms and silicoflagellates, which increase opal fluxes to depth [*Santamaría-del-Angel et al.*, 1994; *Thunell et al.*, 1996]. In summer, weaker winds blow from the southeast, allowing ETNP surface waters to penetrate into the GC and water column stratification to reoccur [*Roden*, 1958; *Badan-Dangon et al.*, 1991]. Summertime nutrient limitation leads to lower biological production and a plankton community structure characterized by coccolithophores and foraminifera, which contribute to enhanced carbonate fluxes [*Brand*, 1994; *Thunell et al.*, 1996; *Ziveri and Thunell*, 2000]. In contrast to seasonal changes in the biomineral fluxes, vertical fluxes of particulate organic carbon and nitrogen remain invariant [*Thunell*, 1998; *Lyons et al.*, 2011; *White et al.*, 2013] and do not correlate with overlying surface productivity, suggesting that export production may be more efficient in the summer than during the winter. One hypothesis for this summertime increase in export efficiency is that the GC biological food web undergoes a fundamental seasonal change.

Upon summer stratification, the ensuing intensification of nitrate limitation and presence of residual phosphate as a consequence of the upwelling of waters with low N/P ratios is consistent with conditions that have been

hypothesized to favor the growth of nitrogen-fixing organisms [*Karl*, 2002]. High rates of N_2 fixation, as well as episodic decreases in the $\delta^{15}N$ value of sinking particulate nitrogen captured in deep sediment traps located in the central GC basins (e.g., Carmen and Guaymas Basin), suggest that diazotrophy may also significantly contribute to the sinking particulate matter flux during the summer period [*Thunell*, 1998; *Altabet et al*., 1999; *White et al*., 2007, 2013]. This variability in food web structure caused by seasonal stratification combined with low oxygen in mid-waters of the GC and adjacent ETNP therefore provides an excellent opportunity to study the linkages between surface productivity and particulate export fluxes under oceanographic conditions similar to those expected in a future warmer ocean.

A method increasingly used to estimate particle flux in marine systems is the measurement of the disequilibrium between naturally occurring thorium-234 ($T_{1/2}$ = 24.1 days) and its long-lived radioactive parent, uranium-238 ($T_{1/2} = 4.47 \cdot 10^9$ years) [*Benitez-Nelson and Moore*, 2006]. ^{238}U is conservative in seawater [*Chen et al*., 1986], while its radioactive daughter, ^{234}Th, is highly particle reactive. As such, ^{234}Th is rapidly scavenged onto particle surfaces and removed when the carrier particles sink, creating disequilibrium between the parent-daughter pair in the upper water column. The value for the integrated deficit of ^{234}Th with respect to ^{238}U in the water column is converted into a flux when multiplied by the ^{234}Th decay constant, thus providing an estimate of the sinking ^{234}Th flux that must have occurred on timescales of weeks to months prior to radionuclide measurement. As such, $^{234}Th/^{238}U$ disequilibria have become a powerful tracer for studying particle formation and export on such timescales [*Coale and Bruland*, 1985; *Cochran and Masqué*, 2003] and are an excellent complement to particle flux estimates from sediment traps [*Buesseler*, 1991]. One of the critical assumptions behind using $^{234}Th/^{238}U$ disequilibria to estimate element flux is the element to ^{234}Th ratio in sinking particles used to convert ^{234}Th fluxes into particulate fluxes for the element of interest. Several authors have highlighted the spatial and temporal variability in element/^{234}Th ratios found in marine systems not only as a function of plankton community structure, particle size distribution, food web dynamics, and aggregation-disaggregation processes, but also as a result of the various methodologies used to sample those sinking particles [e.g., sediment traps, in situ pumps, and bottles] [*Moran et al*., 2003; e.g., *Benitez-Nelson and Charette*, 2004; *Buesseler et al*., 2006].

The goal of this study is to better understand the processes influencing particulate organic carbon, nitrogen, and biogenic silica export in the GC and the ETNP during the stratified summer period when smaller phytoplankton and nitrogen-fixing organisms likely dominate. We used free floating sediment traps and $^{238}U/^{234}Th$ disequilibrium to quantify export fluxes. We further examined how element/^{234}Th ratios collected at high resolution throughout the upper water column influence ^{234}Th-derived particle export results and provide insight into the composition and source of particles contributing to the sinking flux.

2. Methods

Samples were collected at seven stations within the GC and ETNP adjacent waters, with one station (GC4-2) resampled after approximately 6 days (GC4-2b), during July–August 2008 aboard the R/V *New Horizon* (Figure 1). At each station, seawater samples were collected throughout the water column using Niskin bottles. Total ^{234}Th was measured from 4 L of seawater collected at 24 discrete depths over the upper 1000 m. Samples were processed via the MnO_2 coprecipitation technique [*Pike et al*., 2005] and counted onboard using a gas flow proportional low-level RISO beta counter (counting statistics $<$5%). Each was recounted $>$6 months later to determine background activities before processing for chemical recoveries of Th (average recovery = 91 ± 7%, n = 171) by inductively coupled plasma mass spectrometry. ^{238}U activities were calculated from salinity data using the relationship from *Pates and Muir* [2007]. Water column ^{234}Th fluxes (WC fluxes) at various depths were derived from the integrated ^{234}Th deficits with respect to ^{238}U activities.

Sinking particles were collected using VERTEX-style sediment traps (ST) deployed for 24 h at each station. Each ST was equipped with 12 tubes per depth (100 and 105 m), filled with an unpoisoned NaCl brine solution. Three tubes from each depth were used to determine particulate ^{234}Th. The content of each tube was filtered at sea separately onto 25 mm diameter acid-rinsed and precombusted quartz microfiber filters (Whatman, QMA). Swimmers were identified via visual inspection and removed from the filtered sample. Total particulate carbon (PC), particulate organic carbon (POC), and particulate nitrogen (PN) were also determined in the ST material using the methods described in *Benitez-Nelson et al*. [2007] and *White et al*. [2013].

Particlestable isotopic composition (δ^{15}N and δ^{13}C values) was determined using the methods described by *Prahl et al*. [2005].

Particulate samples were also collected at each station from 9 to 13 depths over the upper 500 m using in situ pumps (ISP). Between 400 and 700 L of water was filtered through a 142 mm diameter acid-rinsed 53 μm mesh nitex screen followed by a 142 mm diameter, 1 μm pore-size acid-rinsed, and combusted QMA. Each 53 μm nitex screen was rinsed into a clean plastic beaker using 0.2 μm filtered seawater and mixed with a stirring plate to homogenize the sample. From the rinse, a one-fourth aliquot was filtered onto precombusted 25 mm QMA for direct analysis of ^{234}Th, while the remaining solution was filtered onto precombusted GF/F for analysis of PC, PN, and the stable isotopic composition of both elements (δ^{13}C and δ^{15}N) following the same procedures used for ST samples. The 1–53 μm size fraction was subsampled using ten 21 mm diameter punches (26% of total filter area of the 142 mm diameter QMA) and counted directly for ^{234}Th at sea. Additional punches were analyzed for PC and PN concentrations and C and N isotopic composition. POC was analyzed in selected samples for both size classes. Biogenic silica (bSi) was analyzed from the >53 μm size fraction via wet alkaline digestion following *DeMaster* [1991]. Particulate samples from both the ST and ISP were recounted for background correction more than 6 months after collection.

Profiles of the total beam attenuation coefficient, $c(\lambda)$, and the total absorption coefficient, $a(\lambda)$, were collected at each sampling station with a WetLabs AC-S at 82 wavelengths (400.5–752.7 nm; mean binwidth = 4.3 nm). The absorption spectra of colored dissolved organic matter [CDOM, $a_g(\lambda)$] was measured in parallel with a WetLabs AC-9 (412, 440, 488, 510, 555, 630, 650, 676, and 715 nm) with 0.2 μm cartridge filters attached to the instrument inflow. CDOM spectra were interpolated to AC-S wavelengths. All data were filtered to remove outliers (generally due to bubbles at shallow depths), binned to 1 m, and corrected for in situ temperature- and salinity-dependent variations in absorption and attenuation as per *Twardowski et al*. [1999]. Pure water calibrations were performed every 2 days to ensure there was no instrument drift.

Complementary phytoplankton community structure was obtained by microscopy and pigment analysis using high-performance liquid chromatography (HPLC). Primary production and N_2 fixation rates were also measured using in situ incubations with ^{13}C-labelled bicarbonate and ^{15}N-labelled nitrogen gas additions, respectively. Detailed information regarding these procedures is given in *White et al*. [2013].

3. Results

3.1. Hydrography

Sampled stations were grouped into three subregions based on their hydrographic properties: the ETNP (GC4-10, GC4-11, and GC4-12), the Transition zone (GC4-8 and GC4-9), and the GC (GC4-1 and GC4-2). At the time of sampling, ETNP stations were characterized by cooler (17–24°C) and fresher (salinity ~33.7) surface waters and fresher subsurface waters (to 300 m) associated with California Current Water (CCW) (Figure 1). Deeper waters were composed of California Undercurrent Water (CUCW, GC4-12) and Subtropical Subsurface Water (SSW, GC4-10 and GC4-11), with Pacific Intermediate Waters (PIW) found at depths greater than 500 m [*Lynn and Simpson*, 1987].

Within the GC, stations GC4-1 and GC4-2 were located within two narrow sub-basins: the del Carmen (26°20′N, 110°40′W) and Pescadero Basins (24°00′N, 108°50′W), respectively. Surface waters (0–100 m) were characterized by salty (salinity >34.9) Gulf of California Waters (GCW). Colder deeper SSW waters occurred down to 500 m with even colder waters below the SSW, classified as PIW [*Castro et al*., 2006] (Figure 1). The Transition zone (GC4-8 and GC4-9) was characterized by a mixture of physical regimes, with upper waters dominated by Tropical Surface Waters (TSW). Deep Pacific Waters (DPW) were only observed at the deepest sampled depth (3000 m) at station GC4-8.

The study area was characterized by oligotrophic conditions, with surface layers (upper 20 m) containing N-poor and P-replete concentrations (0.03–0.09 μmol L^{-1} for nitrate + nitrite and 0.3–0.8 μmol L^{-1} for phosphate) [*White et al*., 2013]. Warm and salty surface waters cooled and freshened as they moved out of the GC and northward along the ETNP transect. Mixed layer depths also deepened along with the depth of the euphotic zone (Ez), defined here as the depth of 0.1% light penetration [as in *Buesseler and Boyd*, 2009] and determined using profile data from a photosynthetically active radiation sensor on the

Table 1. Euphotic Zone Depth, Net Primary Production, ^{234}Th Fluxes, and Elemental/^{234}Th Ratios[a]

Station	Ez (m)	NPP (mmol C m^{-2} d^{-1})	^{234}Th fluxes (dpm m^{-2} d^{-1})		ST ratios		SP ratios		LP ratios		
			Sediment Trap	Water Column	PC/^{234}Th µmol/dpm	PN/^{234}Th µmol/dpm	PC/^{234}Th µmol/dpm	PN/^{234}Th µmol/dpm	PC/^{234}Th µmol/dpm	PN/^{234}Th µmol/dpm	bSi/^{234}Th µmol/dpm
GC4-1	75	67 ± 10	6300 ± 1030	2600 ± 200	5 ± 1	0.7 ± 0.1	2.4 ± 0.3	0.38 ± 0.04	1.59 ± 0.04	0.182 ± 0.005	0.27 ± 0.01
GC4-2	90	34 ± 3	4900 ± 570	3400 ± 140	5.5 ± 0.7	0.7 ± 0.1	3.1 ± 0.3	0.50 ± 0.05	1.4 ± 0.1	0.14 ± 0.01	0.039 ± 0.004
GC4-2b	75	32 ± 3	2600 ± 340	NA	9 ± 2	1.2 ± 0.3	5.1 ± 0.6	0.84 ± 0.09	2.3 ± 0.2	0.26 ± 0.02	0.16 ± 0.01
GC4-8	110	31 ± 3	3500 ± 340	1400 ± 170	16 ± 5	2.2 ± 0.6	3.9 ± 0.4	0.78 ± 0.08	1.9 ± 0.2	0.23 ± 0.02	0.064 ± 0.006
GC4-9	80	27 ± 5	2000 ± 330	1100 ± 210	6 ± 1	0.7 ± 0.2	1.3 ± 0.1	0.22 ± 0.02	1.0 ± 0.1	0.11 ± 0.01	0.011 ± 0.001
GC4-10	95	47 ± 4	3100 ± 450	900 ± 220	5.6 ± 0.7	0.8 ± 0.1	2.3 ± 0.3	0.30 ± 0.03	1.8 ± 0.2	0.16 ± 0.02	0.11 ± 0.01
GC4-11	100	30 ± 4	1400 ± 170	1700 ± 190	11 ± 1	1.1 ± 0.1	2.7 ± 0.2	0.44 ± 0.03	1.6 ± 0.1	0.12 ± 0.01	0.12 ± 0.01
GC4-12	90	117 ± 8	1700 ± 170	1900 ± 150	13 ± 2	1.6 ± 0.3	2.4 ± 0.2	0.35 ± 0.03	1.79 ± 0.09	0.18 ± 0.01	0.47 ± 0.02

[a]Euphotic zone depth (Ez) defined as 0.1% light level. Net primary production (NPP) was integrated over the upper 60 m. ^{234}Th fluxes were calculated at 100 m. Elemental/^{234}Th ratios from the different particulate material collected at 100 m (ST = sediment trap; SP = ISP small particles; LP = ISP large particles, see text for details). NA is noted when samples were not available.

conductivity-temperature-depth rosette (Table 1). This depth is where ^{234}Th was found to be in equilibrium with ^{238}U at the majority of stations sampled (Figure 2).

3.2. ^{234}Th and ^{238}U Profiles and ^{234}Th Fluxes

Total ^{234}Th activities ranged from 0.8 to 2.8 dpm L^{-1} (Figure 2), with particulate ^{234}Th activities (Table S1 of the supporting information) in the small particles (1–53 µm) accounting for 4% to 33% of the total activity measured (average 14 ± 6%). ^{234}Th activities in large particle (>53 µm) accounted for a smaller fraction of the total ^{234}Th activity, averaging 5 ± 4% with a range of 0.4% to 17%.

A deficit of ^{234}Th with respect to ^{238}U over the upper 100 m was observed at all stations (Figure 2). The magnitude of this deficit, however, was greater within the GC, where ^{234}Th disequilibrium was found to depths of 700 and 300 m at stations GC4-1 and GC4-2, respectively. Excess ^{234}Th activity was only measured between 80 and 250 m (average 0.25 ± 0.05 dpm L^{-1}) in the most northern station of the ETNP sampling region (GC4-12), representing almost 60% of the ^{234}Th deficit measured in the upper 100 m.

^{234}Th fluxes obtained from ST at 100 and 105 m were in excellent agreement (average factor 1.04 ± 0.13). We therefore focus on ST results collected at 100 m, which is a commonly used depth, to estimate particle fluxes found in the literature. The WC-derived ^{234}Th fluxes were obtained by integrating the ^{234}Th deficit over the upper 100 m using a steady state one-dimensional model. Both the ST- and the WC-derived ^{234}Th fluxes are presented in Table 1 and Figure 3. WC fluxes at 100 m, which ranged from 890 ± 220 to 3400 ± 140 dpm m^{-2} d^{-1}, were in excellent agreement with those obtained directly from the ST (ratios between both estimates averaged 0.9 ± 0.1) at the most northern stations of the ETNP (GC4-11 and GC4-12). At the remaining stations, ST fluxes at 100 m ranged from 1400 ± 170 to 6300 ± 1000 dpm m^{-2} d^{-1} and are thus 1.4 to 3.5 times higher (average 2.3 ± 0.8) than those derived from the WC. Both methods yielded larger fluxes within the interior of the GC. At the reoccupation of station GC4-2 (GC4-2b), 6 days after the first sampling, ST ^{234}Th flux decreased by almost 50%, from 4900 ± 570 to 2600 ± 340 dpm m^{-2} d^{-1}, which highlights the short timescale of ST measurements compared to WC ^{234}Th deficits.

3.3. Particle Distribution and Composition

3.3.1. Particle Size Distribution Analysis

The particulate beam attenuation coefficient, $c_p(\lambda)$, was calculated by subtraction of CDOM absorption, $a_g(\lambda)$, from $c(\lambda)$. The general shape of the spectra of beam attenuation $c_p(\lambda)$ is well approximated by a power law as follows [*Bricaud et al.*, 1998]:

$$c_p(\lambda) = c_p(\lambda_0)(\lambda/\lambda_0)^{-\gamma_{cp}} \quad (1)$$

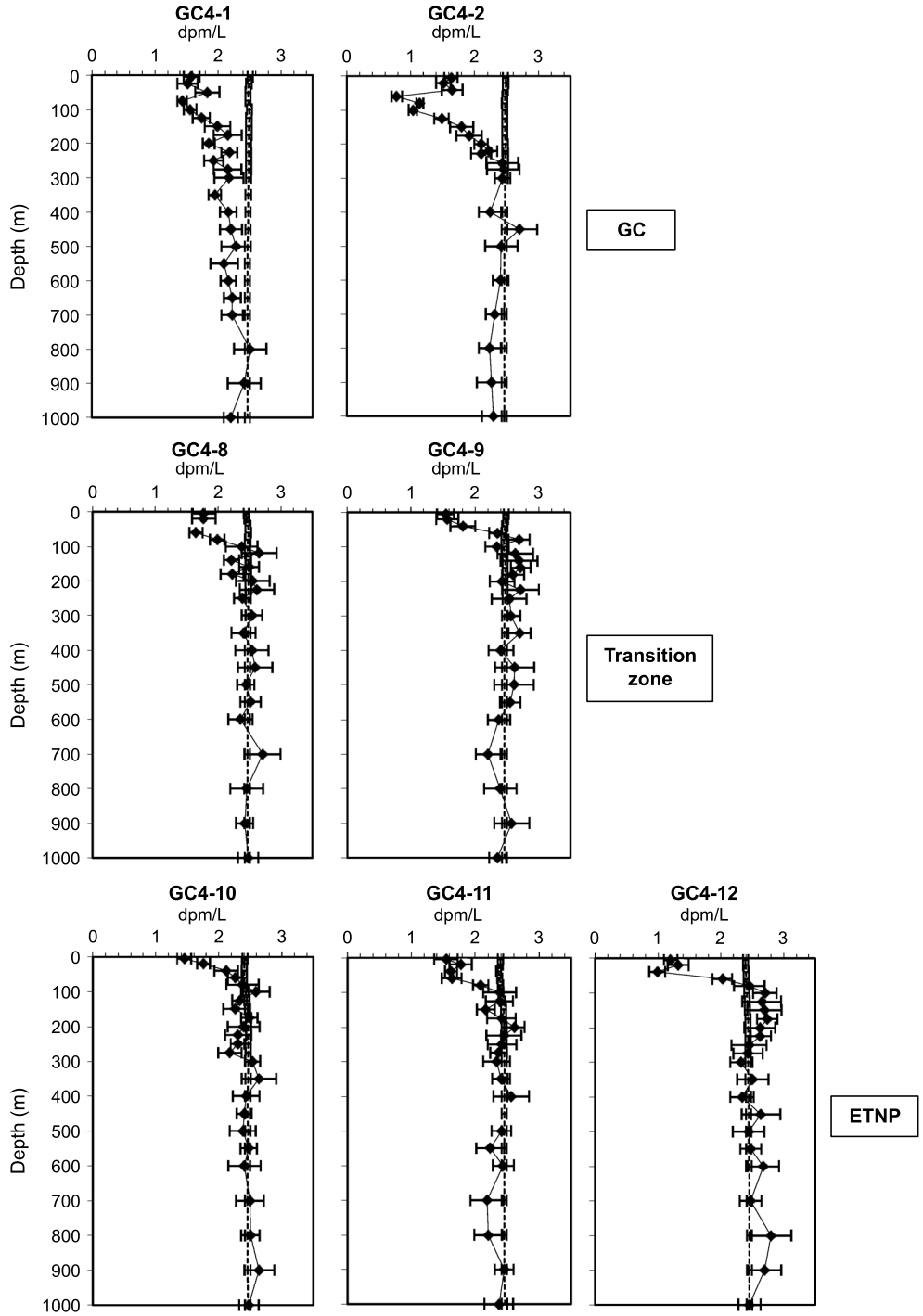

Figure 2. ^{234}Th (black diamonds) and ^{238}U (dashed line) concentration profiles down to 1000 m obtained at each station. ^{238}U concentrations were calculated using the U-Salinity relationship from *Pates and Muir* [2007]. The profiles are presented in the three groups corresponding to GC stations (GC4-1 and GC4-2), Transition zone stations (GC4-8 and GC4-9), and ETNP stations (GC4-10, GC4-11, and GC4-12).

The magnitude of the particle beam attenuation coefficient at 660 nm, $c_p(660)$, is to a first order proportional to the concentration of suspended particles [*Gardner et al.*, 2006], whereas its spectral slope, γ_{cp}, is related to the slope of the particle size distributions (PSD) under certain assumptions by $\xi = \gamma_{cp} + 3$ [*Kostadinov et al.*, 2012]. γ_{cp} was calculated using ordinary least squares regression on the log-transformed

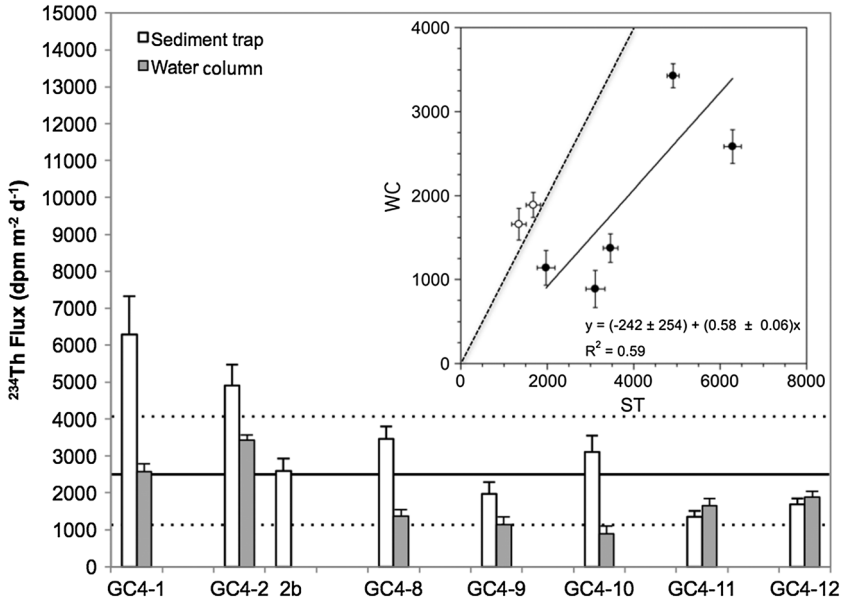

Figure 3. Sediment trap (ST) (open bars) and water column (WC) (grey bars) derived ^{234}Th fluxes at 100 m. Solid line indicates average fluxes, considering direct fluxes from the sediment trap and water column-derived fluxes. Dashed lines indicate the standard deviation. The inset figure represents WC-derived ^{234}Th fluxes (dpm m^{-2} d^{-1}; *y* axis) versus ST fluxes (dpm m^{-2} d^{-1}; *x* axis). Open circles correspond to stations GC4-11 and GC4-12, and closed circles correspond to the remaining stations. The solid line and equation indicate the linear regression for the closed circles. The dashed line indicates the ideal 1:1 relationship between the sediment trap and water column-derived fluxes.

data within 440–676 nm. Larger values of ξ, i.e., steeper slopes, indicate higher abundance of small particles. The percent contribution of picoplankton (0.5–2.0 μm), nanoplankton (2.0–20 μm), and microplankton (20–50 μm) to total particle volume was then calculated according to *Kostadinov et al.* [2010, equation (1)]. It is important to highlight that the slope of the beam attenuation profile used to obtain particle size classes is based on the scattering of particles without discriminating live particles from detritus.

PSD profiles (Figure 4) clearly reflect a decline in the relative contribution of small particles as we transited out of the GC into the transition zone and into the ETNP. To link these changes to the size structure of the phytoplankton community structure we refer to the HPLC data presented in *White et al.* [2013]. HPLC-based estimates of cell size use the relative proportion of diagnostic pigments to estimate the contributions of picophytoplankton (<2 μm), nanophytoplankton (2–20 μm), and microphytoplankton (20–200 μm) and make simplifying assumptions about the size classes associated with each pigment considered. Therefore, both approaches provide independent estimates of particle size distributions. While the absolute size distributions differ between techniques and is to some extent expected given that these methods are fundamentally measuring different properties (e.g., the slope of scattering spectra and pigment ratios), they both show a measurable shift in particle size from smaller particles to larger particles across the transition zone from the GC into the ETNP.

3.3.2. Elemental Composition

The PC and PN concentrations in particles collected with the ISP ranged from 0.2 to 3.4 μmol C L^{-1} and 0.03 to 0.55 μmol N L^{-1} for small particles (1–53 μm) and 0.03 to 2.6 μmol C L^{-1} and 0.002 to 0.34 μmol N L^{-1} for large particles (>53 μm) (Table S1). Small particles accounted for the bulk of the PC and PN, averaging 85 ± 9% and 89 ± 11% of the total particulate pool, respectively. Depth patterns were similar between the two size classes at all stations. Maximum PC and PN concentrations were typically located between 20 and 50 m, and decreased by as much as a factor of 10 down to a depth of 500 m. The PC/PN ratios showed little change with depth, averaging 7 ± 1 in small particles, while the average PC/PN ratio in large particles was significantly higher (10 ± 2) ($p < 0.0001$; $n = 165$). Inorganic carbon was minimal in both size fractions, with no significant differences between PC and POC (average factor

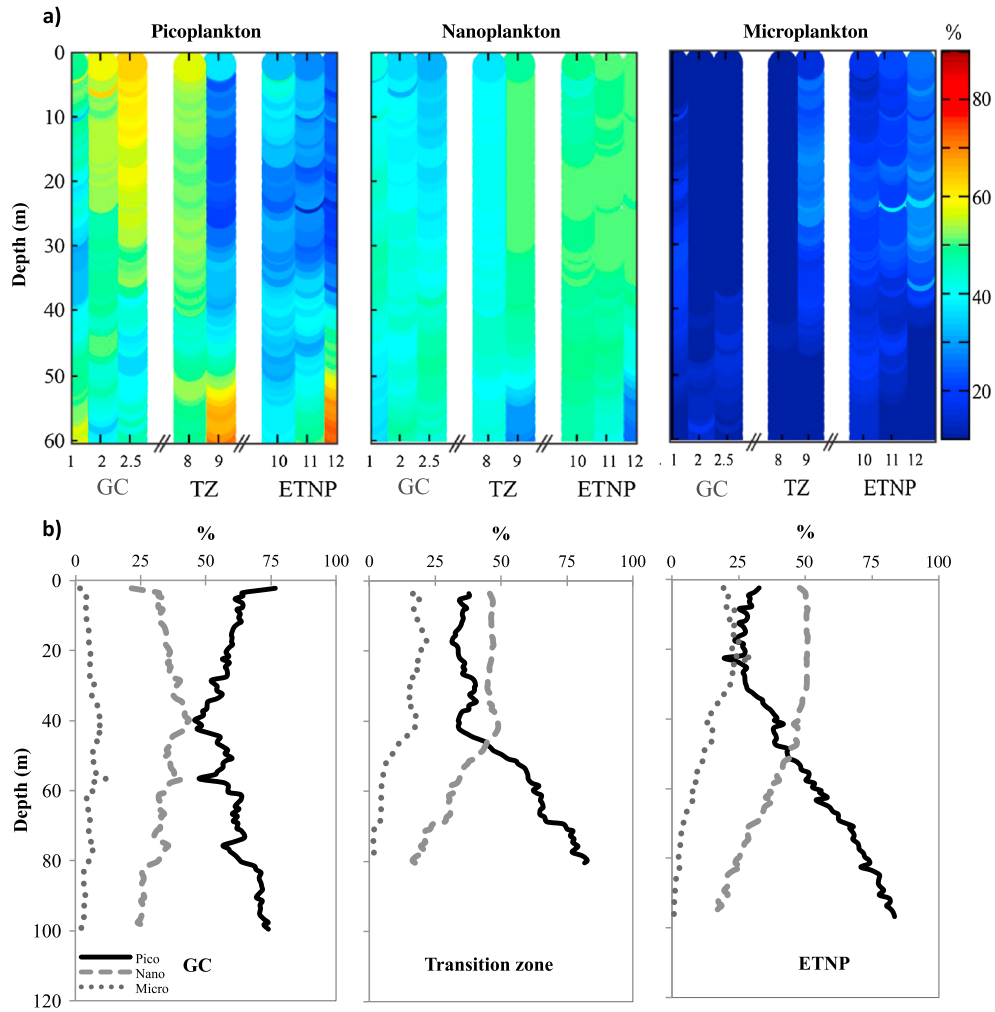

Figure 4. (a) Particle size distribution profiles for pico-, nano-, and microplankton abundances obtained at each station and (b) averaged particle size distribution profiles grouped by regions: GC, Transition zone, and ETNP. Profiles of Figure 4a are cropped to a depth of 60 m for simpler comparison to HPLC data from [*White et al.*, 2013, Figure 6].

difference 1.1 ± 0.1, $n = 20$, for small particles, and 1.0 ± 0.2, $n = 16$, for large particles). Carbon content within the ST material was also dominated by POC (average factor difference between PC and POC 1.3 ± 0.3, $n = 8$), with an average PC/PN ratio of 8 ± 1 ($n = 8$).

3.3.3. Stable Isotopic Composition

δ^{15}N and δ^{13}C values were measured on particles collected at each station (Table S1). Profiles of δ^{15}N values were relatively constant over the upper 100 m with no significant difference between the ISP small and large particles ($p > 0.1$; $n = 100$; δ^{15}N = 9.6 ± 1.8‰). In contrast, the δ^{13}C values of small and large ISP particles were significantly different throughout the water column, with smaller particles averaging −22.0 ± 1.2‰ and large particles averaging −20.1 ± 0.8‰ over the upper 100 m ($p < 0.0001$ in both cases; $n = 102$ for samples above 100 m and $n = 66$ for deeper samples). There were no significant differences between the δ^{15}N of ST and ISP samples from the upper 100 m ($p > 0.5$ for both size classes). However, significant differences were apparent between the δ^{13}C of ST (−21.8 ± 1.3 ‰; $n = 8$) and large ISP particles ($p < 0.0001$; $n = 60$), whereas no differences were observed between the δ^{13}C values of ST and small ISP particles.

3.3.4. Elemental/^{234}Th Ratios

Elemental ratios of PC and PN to ^{234}Th collected using the ISP were higher in the small versus large size classes over the upper 100 m but converged with increasing depth at 200–500 m (Figure 5). The PC/^{234}Th

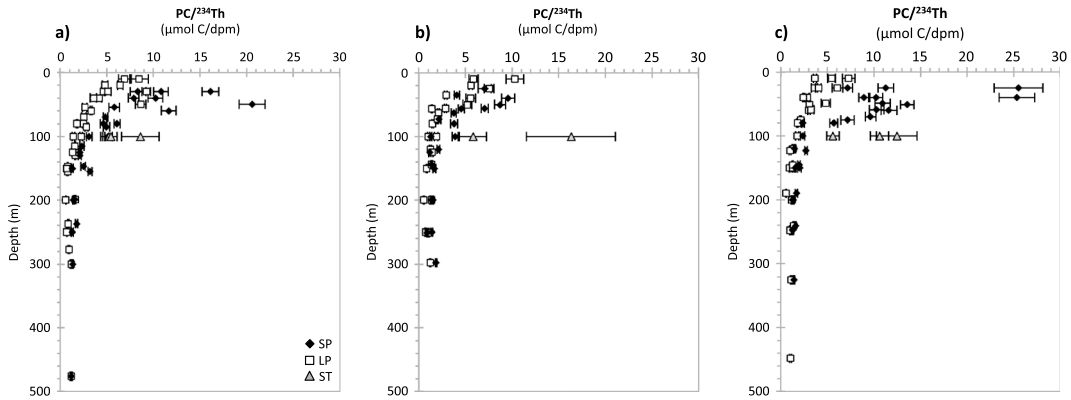

Figure 5. Particulate PC/^{234}Th ratio profiles at (a) the GC stations (GC4-1, GC4-2, and GC4-2b), (b) the Transition zone stations (GC4-8 and GC4-9), and (c) the ETNP stations (GC4-10, GC4-11, and GC4-12), obtained with the in situ pumps from small particles (SP) (black diamonds) and large particles (LP) (open squares). Ratios measured in the sediment traps (ST) are presented as grey triangles. Small particles were only plotted below 20 m due to subsurface maxima located at that depth.

ratios of small and large particles measured at 100 m were on average lower than the ratios obtained from the ST by a factor of 3.2 ± 1.4 and 5.8 ± 2.8, respectively (Table 1). The magnitude of this difference varied both regionally and with particle size, with station GC4-8 and the northernmost stations of the ETNP showing the largest contrast. PN/^{234}Th ratios followed a similar trend (Table 1). Close examination of the data shows that the elemental to ^{234}Th ratios measured in ST samples at 100 m are much more comparable to those measured in both ISP-collected size classes at the surface (Figure 5). The bSi/^{234}Th ratios measured in the large size fraction of particulate material collected with the ISP ranged from 0.12 to 0.45 µmol dpm^{-1}, with the highest values measured at stations GC4-1 and GC4-12 (Table 1).

3.3.5. Attenuation Analysis

The high resolution of the ISP sampling along the water column allows us to estimate a net attenuation term, *b*, which indicates how rapidly PC and PN are attenuated relative to ^{234}Th; e.g., larger absolute *b* values imply higher attenuation rates. Similar to the commonly used Martin curve, applied to evaluate the particle flux attenuation with depth [*Martin et al.*, 1987], the *b* term was obtained from a power regression of PC and PN to ^{234}Th ratios versus depth throughout the water column at each station [equation (2) and Figure 5], such that

$$\mathrm{PC}/^{234}\mathrm{Th} = \mathrm{PC}/^{234}\mathrm{Th}_{\mathrm{o}} \cdot (Z/Z_{\mathrm{o}})^{-\mathrm{b}} \tag{2}$$

where PC/^{234}Th$_o$ is the term obtained from the fitting using least squares regression that represents the PC/^{234}Th ratio at the base of the euphotic zone (µmol dpm^{-1}), Z is the depth at which we calculate the PC/^{234}Th ratio, and Z_o is the depth of the euphotic zone. The same equation can be applied to PN/^{234}Th ratios.

Element to ^{234}Th ratios measured in large and small ISP particles were plotted separately to examine possible size-dependant differences in attenuation profiles (Figure 5). The results indicate that PC and PN in small particles are attenuated at a significantly faster rate relative to ^{234}Th with depth, with *b* terms for small particles being 0.66 and 0.76 for PC and PN, respectively, compared to 0.39 and 0.65 for large particles (Kolmogorov-Smirnov test $p < 0.0001$; $n = 88$ for both data sets, PC and PN).

3.4. PC, PN, and bSi Fluxes

The absolute magnitude of PC and PN fluxes at 100 m (Figure 6 and Table 2) was determined directly using ST and indirectly from the WC-derived ^{234}Th fluxes using station-specific ST and ISP element/^{234}Th ratios presented in Table 1. The magnitude of the derived elemental fluxes was strongly driven by the elemental/^{234}Th ratio used (i.e., ST ratio > small particle ratio > large particle ratio). Although ^{234}Th fluxes obtained from ST varied considerably (~50% decrease) over relatively short time periods (<7 days) at

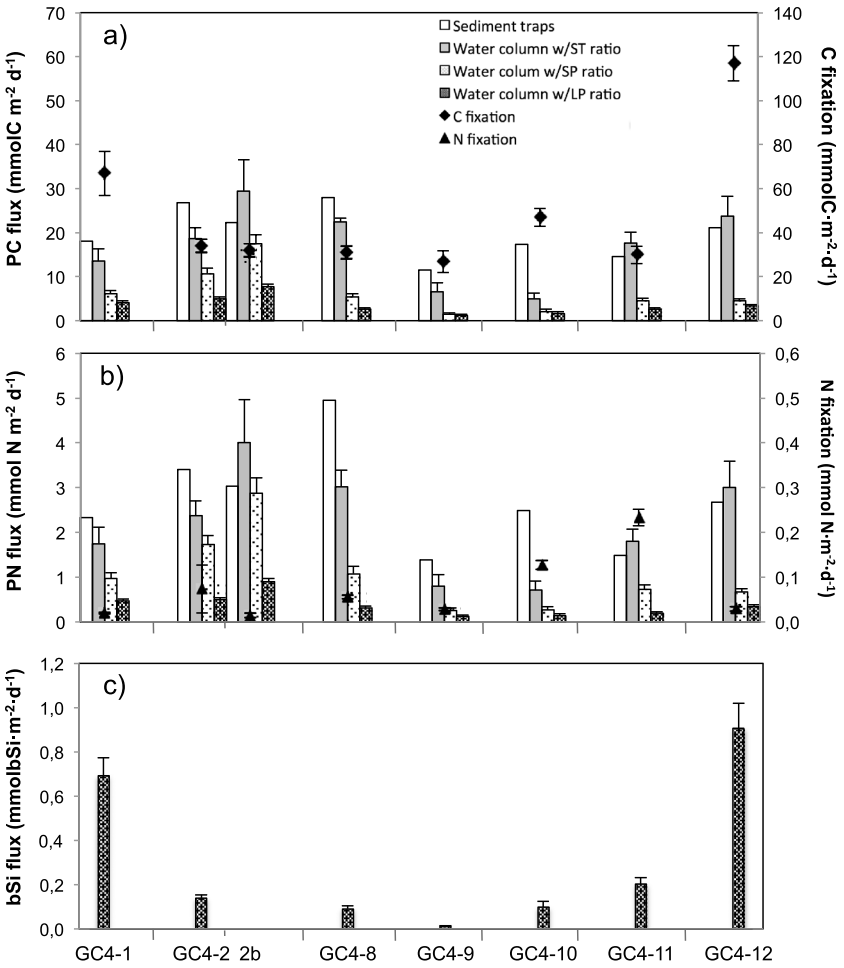

Figure 6. ^{234}Th-derived fluxes and direct measurements by sediment traps at 100 m. The legend depicted in Figure 6a is the same for all plots. (a) PC fluxes (bars) together with C fixation rates integrated over the upper 60 m (black diamonds); (b) PN fluxes (bars) together with N fixation rates integrated over the upper 60 m (black triangles). Please note the different scales when comparing PC flux and C fixation and PN flux and N fixation. (c) bSi fluxes. C and N fixation data obtained from *White et al*. [2013]. GC4-2b-derived fluxes were calculated using the water column ^{234}Th flux from GC4-2 and the element to ^{234}Th ratios from GC4-2b.

station GC4-2, such changes were not clearly reflected in the PC and PN fluxes due to the PC(PN)/^{234}Th variation (~50% increase).

Elemental fluxes obtained directly with the ST and by means of WC ^{234}Th deficits using the elemental ratios obtained from ST were in relatively good agreement. ST fluxes were higher by an average factor of 1.5 ± 0.9 for PC fluxes and 1.6 ± 0.9 for PN fluxes at all stations, except at GC4-2b and at the northernmost ETNP station (GC4-12). As mentioned previously, values for elemental/^{234}Th ratios tended to be higher in small versus large particles but converged with increasing depth. As a result, PC and PN fluxes at 100 m derived using WC ^{234}Th deficits and ratios measured on small and large particles agreed within a factor of 1.8 ± 0.6 for PC and 2.7 ± 0.8 for PN. In contrast, when fluxes estimated using ST elemental/^{234}Th ratios are compared with those estimated using ISP data, we find that the former were always higher, ranging from a factor of 1.7 to 10 for PC (average 3.2 ± 1.4 and 5.8 ± 2.8 for small and large particles, respectively) and from a factor of 1.3 to 10 for PN (average 2.5 ± 1.0 and 6.5 ± 2.4 for small and large particles, respectively). Fluxes estimated using PC and PN to ^{234}Th ratios for the combined small and large ISP particles were in agreement with ST fluxes within a factor of 2–4. These particle flux estimates highlight the large variability that occurs as a consequence of the different element/^{234}Th ratios used.

Table 2. Summary of Particulate C, N, and bSi Fluxes and Export Efficiencies[a]

Station	PC Fluxes mmol C m^{-2} d^{-1}				PN Fluxes mmol N m^{-2} d^{-1}				bSi Fluxes mmol Si m^{-2} d^{-1}		*ThE* Ratios 100 m			Exp Eff 100 m Below Ez						
														SP				LP		
	ST	ST Ratio	SP Ratio	LP Ratio	ST	ST Ratio	SP Ratio	LP Ratio	LP Ratio	ST	ST Ratio	SP Ratio	LP Ratio	Ez Ratio[c]	T_{100}[d]	Eff[e]	Ez Ratio[c]	T_{100}[d]	Eff[e]
GC4-1	18	14 ± 3	6.1 ± 0.8	4.1 ± 0.3	2.3	1.8 ± 0.4	1.0 ± 0.1	0.47 ± 0.04	0.70 ± 0.06	27%	20%	9%	6%	0.14	0.80	11%	0.07	1.34[f]	9%
GC4-2	27	19 ± 3	11 ± 1	4.9 ± 0.5	3.4	2.4 ± 0.3	1.7 ± 0.2	0.50 ± 0.05	0.13 ± 0.01	79%	55%	31%	14%	0.49	0.54	27%	0.24	0.53	12%
GC4-2b[b]	22	30 ± 7	18 ± 2	7.7 ± 0.6	3.0	4.0 ± 1.0	2.9 ± 0.3	0.90 ± 0.07	NA	70%	92%	55%	24%	0.62	0.37	23%	0.11	0.55	11%
GC4-8	28	22.3 ± 0.8	5.4 ± 0.8	2.6 ± 0.4	4.9	3.0 ± 0.4	1.1 ± 0.2	0.31 ± 0.05	0.09 ± 0.01	90%	72%	17%	8%	0.14	0.55	7%	0.07	0.40	3%
GC4-9	12	7 ± 2	1.5 ± 0.3	1.2 ± 0.2	1.4	0.8 ± 0.3	0.3 ± 0.1	0.12 ± 0.03	0.012 ± 0.002	43%	25%	6%	4%	0.10	0.41	4%	0.09	0.45	4%
GC4-10	17	5 ± 1	2.1 ± 0.6	1.6 ± 0.4	2.5	0.7 ± 0.2	0.3 ± 0.1	0.14 ± 0.04	0.09 ± 0.03	37%	11%	4%	3%	0.05	0.77	3%	0.03	0.63	2%
GC4-11	15	18 ± 3	4.5 ± 0.6	2.6 ± 0.3	1.5	1.8 ± 0.3	0.7 ± 0.1	0.27 ± 0.04	0.19 ± 0.03	49%	59%	15%	9%	0.27	0.29	8%	0.09	0.84	7%
GC4-12	21	24 ± 4	4.5 ± 0.5	3.4 ± 0.3	2.7	3.0 ± 0.6	0.7 ± 0.1	0.34 ± 0.03	0.89 ± 0.08	18%	20%	4%	3%	0.04	0.51	2%	0.03	0.23	1%

[a]Fluxes obtained directly from the sediment traps (ST) or derived from the water column ^{234}Th deficits at 100 m using sediment trap ratios (ST ratio), in situ pump small particles (SP ratio), or large particles (LP ratio) (see text for details). *ThE* ratios were calculated using the four approaches to estimate PC fluxes at 100 m. Export efficiencies 100 m below the euphotic zone are also presented, together with Ez-ratio and T_{100} values. NA is noted when samples were not available.
[b]GC4-2b derived fluxes were obtained calculated using the water column ^{234}Th flux form GC4-2 and element to ^{234}Th ratios from GC4-2b.
[c]Ez ratio = PC flux at Ez : NPP.
[d]T_{100} = PC flux 100 m below Ez : POC flux at Ez.
[e]Eff = Ez ratio * T_{100}.
[f]$T_{100} > 1$ due to high PC flux at attenuation depth as a consequence of a ^{234}Th deficit below Ez and low PC/^{234}Th ratio at the attenuation depth.

Fluxes of bSi estimated from WC ^{234}Th deficits and values for bSi/^{234}Th ratios measured in ISP large particles were only significant where microscopy and pigment composition indicated a diatom-dominated community structure [*White et al.*, 2013]: at stations GC4-12 (0.91 ± 0.11 mmol bSi m^{-2} d^{-1}) and GC4-1, below the nitracline (30 m), (0.69 ± 0.07 mmol bSi m^{-2} d^{-1}). At all other locations, where a picocyanobacterial-dominated community structure was observed (Figure 4; *White et al.* [2013]), bSi fluxes were 0.01–0.20 mmol bSi m^{-2} d^{-1}.

4. Discussion

A major goal of this study was to examine particle export within the ETNP and GC in response to overlying water column productivity and community composition and to use these results as an analog for understanding other stratified tropical ecosystems. Previous work in the GC found that PC and PN fluxes to depth remain fairly constant [winter (Nov–Feb) and summer (Jun–Sep) average export fluxes at ~500 m were not significantly different; 19 ± 4 versus 21 ± 3 mg C m^{-2} d^{-1}, $p > 0.5$], even though primary productivity rates are significantly higher during the winter months (~2 mg m^{-3} versus < 0.5 mg m^{-3}) [*Thunell*, 1998; *Lyons et al.*, 2011; *White et al.*, 2013]. This observation suggests that the export efficiency in summer is greater than in winter. Several studies have suggested that N_2 fixation may enhance PC and PN export fluxes in the North Pacific subtropical gyre [*Scharek et al.*, 1999; *Dore et al.*, 2002] and recent work in the GC region indicates that N_2 fixation may be significant during the stratified summer period when nutrients have been depleted [*White et al.*, 2007]. Such trends remain enigmatic, however, as the temporal and spatial variability in N_2 fixation in this area (from 14 to 795 μmol N m^{-2} d^{-1}) [*White et al.*, 2013] appears to be too large to explain the relatively uniform PC export observed throughout the year.

We have used ^{234}Th as a tracer to estimate particle fluxes within the ETNP and GC during the summer of 2008. This approach has been widely employed to examine episodic events that may be missed using ST

due to temporal constraints and potential methodological issues [e.g., *Buesseler et al*., 1992, 2007]. The application of the ^{234}Th method, however, also requires a number of assumptions, including the determination of the element/^{234}Th ratio necessary to convert ^{234}Th fluxes into the elemental flux of interest. Therefore, we also examine the approaches used in the collection and application of element/^{234}Th ratios and discuss these results in light of regional variability in particle flux and the efficiency of the biological pump in the GC region and the ETNP adjacent waters.

Our overall assessment concludes that small particles are significant contributors to particle flux throughout the GC and ETNP in summer and that export efficiencies in stations dominated by picoplankton containing diazotrophs are higher than in those stations where diatoms were more abundant, confirming the inference from moored sediment traps from *Thunell* [1998] and agreeing with previous work from *Dunne et al*. [1999] who found that nondiatom production was responsible for the majority of the export. When examined on a global perspective, our results further suggest that the phenomenon is not unique to our study region but may apply broadly to ecosystems dominated by smaller taxa, agreeing with previous work from oligotrophic regions [e.g., *Richardson and Jackson*, 2007; *Durkin et al*., 2015]. While others have shown that choosing a single particle fraction to estimate vertical export may be misleading [*Dunne et al*., 1997; *Burd et al*., 2007; *Stewart et al*., 2011], sampling uniquely large particles (>50 μm) is still the dominant approach used to estimate elemental fluxes derived from the ^{234}Th method. Our data again support further discussion of particle size, providing results that indicate the importance of the ecosystem and biological state of the region under interest.

4.1. ^{234}Th Deficits and Fluxes

In this study, ^{234}Th deficits mainly occurred over the upper 100 m, with little evidence of excess ^{234}Th at depth that would imply extensive particle remineralization [*Bacon et al*., 1996; *Buesseler et al*., 2008; *Maiti et al*., 2010]. Our high-resolution sampling suggests that either the remineralization rates were too low to show a clear ^{234}Th excess peak or, if such a peak existed, it was not resolvable within the sampling depth intervals chosen at our stations [e.g., *Maiti et al*., 2010]. Within the GC, ^{234}Th deficits reached depths of 700 m (GC4-1) and 300 m (GC4-2). Water column-derived ^{234}Th fluxes at 100 m at those stations (>2500 dpm m^{-2} d^{-1}) are comparable to other productive coastal regions or to those found during the North Atlantic Bloom Experiment [e.g., *Coale and Bruland*, 1985; *Buesseler et al*., 1992]. Indeed, the fluxes of ^{234}Th obtained from the GC ST at 100 m (≥5000 dpm m^{-2} d^{-1}) are among the highest measured of all previous WC ^{234}Th flux assessments globally [i.e., the maximum flux reported previously was of 5500 dpm m^{-2} d^{-1} for the mid and late SW Monsoon in the Arabian Sea by *Buesseler et al*., 1998. See summary by *Le Moigne et al*., 2013]. Although this comparison should be taken cautiously due to the use of different methods (i.e., ST versus WC fluxes), it helps to highlight the high ^{234}Th fluxes observed at the stations located within the GC. We hypothesize that those stations are influenced by the lateral advection of water and particles from the nearshore due to their location within two narrow basins (Figure 1), as suggested by other studies using longer-lived radionuclides [*Smoak et al*., 1999] and transmissometry profiles (data not shown). Since the total ^{234}Th activity is dominated by the dissolved phase, water from the margins would be expected to have low total ^{234}Th activity from high particle scavenging. Any laterally advected particles would further promote ^{234}Th scavenging, explaining the deep deficits in total ^{234}Th, and they would also increase the particulate ^{234}Th collected by the ST.

Differences between the methodologies used to determine ^{234}Th fluxes (directly from the ST or integrating the WC ^{234}Th deficits) were within a factor of 2 to 4 (average difference of 2.3 ± 0.8), consistent with that typically found in the literature when comparing these collection techniques. These differences may be explained, in part, by the timescale of collection as well as methodological issues: Deficits of ^{234}Th in the water column over the upper 100 m integrate over several weeks, thereby diluting episodic events of higher (or lower) particle fluxes that may have been observable using more short-term deployments, such as the VERTEX-style traps used here [*Buesseler*, 1991]. ST, on the other hand, can be affected by large-scale turbulence and horizontal currents that potentially produce both under- and overcollection biases [*Gardner*, 2000], although the VERTEX-style traps used in this study were designed to minimize this issue [*Hargrave and Burns*, 1979; *Gardner*, 1980].

4.2. Elemental/^{234}Th Ratios

One of the key issues in determining elemental fluxes from ^{234}Th disequilibria is measuring the element to ^{234}Th ratio of sinking particles. These ratios change spatially and temporally depending on the structure of

the plankton community and food web dynamics, but also on the particle collection device used, such as ST and ISPs [*Buesseler et al*., 2006]. Here we explored differences in the element/^{234}Th ratios obtained using these two techniques, considering methodological issues, sinking velocity, and particle size and composition.

4.2.1. Methodological Issues

The disagreement in PC/^{234}Th ratios between ST and large (>53 μm) ISP particles has been observed in several studies [see review by *Buesseler et al*., 2006] and is usually within a factor of 2 to 4 [e.g., *Buesseler et al*., 1992 (North Atlantic Bloom Experiment, JGOFS); *Buesseler et al*., 1995; *Bacon et al*., 1996; *Murray et al*., 1996 (Equatorial Pacific); *Benitez-Nelson et al*., 2001 (North Pacific Subtropical Gyre); *Stewart et al*., 2007 (Mediterranean Sea); *Lepore et al*., 2009 (Mediterranean Sea and Northwest Atlantic)], but may differ by over an order of magnitude, as reported by *Lalande et al*. [2008] for the Barents Sea. Evidence suggests that ISP and ST sample different types of particles depending on their settling velocity. ST tend to undercollect slower sinking particles due to hydrodynamic discrimination [*Gustafsson et al*., 2004], while fast sinking particles are more likely missed by ISP [*Lepore et al*., 2009]. Another issue is that size is not necessarily related to density, and ISP sampling may include communities dominated by large, C-rich neutrally buoyant phytoplankton (i.e., nonsinking but with high PC/^{234}Th ratios) [*Lalande et al*., 2008].

Although the two sampling devices collect fundamentally different particle pools (ST particles represent an average particle size class with respect to flux, whereas ISPs collect particles that represent an average with respect to concentration), sampling biases such as swimmers in ST or the rupture of aggregates by ISPs may further exacerbate these differences. Swimmers have been previously reported as an important source of bias in the PC/^{234}Th ratio of ST if they are improperly removed, since they have a relatively high PC content relative to ^{234}Th [*Coale*, 1990; *Buesseler et al*., 1994]. In this study, obvious swimmers were removed from particulate samples in both types of samples, ST and ISP. However, they may have altered the particle composition during the 24 h ST deployment period via feeding and cell lysis. Indeed, PC and PN fluxes obtained from ST at 100 and 105 m were in good agreement but were more variable (ratios of fluxes at 100 and 105 m were 0.9 ± 0.4 for PC and 1.1 ± 0.3 for PN) than ^{234}Th fluxes (1.0 ± 0.1).

Another possible methodological issue may be related to the rupture of aggregates using ISP. *Gardner et al*. [2003] suggested that lower POC/^{234}Th ratios in ISP samples can result from the rupture of fragile high C concentration particles [e.g., transparent exopolymer particles (TEP) and bacteria] due to the high cross-filter pressure differentials created within an ISP. This would preferentially reduce PC retention. To our knowledge, however, there is no information regarding high TEP concentrations in the study area, nor an anomalous abundance of bacteria, although microscopy of the ST material showed the presence of marine snow [*White et al*., 2013]. The loss of large C-rich particles could also occur due to washout when using ISP. *Bishop et al*. [2012] reported preferential loss of biogenic elements from the >51 μm size fraction when sampling with the most commonly used 142 mm filter holders for ISP. In that study, the values for the ratio of POC to ^{234}Th were not systematically compared between filter holder types, but a few *ad hoc* comparisons suggest that the loss of biogenic material was mirrored by an equivalent loss of particulate ^{234}Th activity (K. Maiti, pers. communication). Therefore, the observed differences in the PC/^{234}Th ratios between large ISP particles and ST in this study do not seem related to the type of filter holder used.

4.2.2. Particle Size, Composition, and Attenuation

Several studies have documented a trend of increasing PC/^{234}Th ratios with increasing particle size as a function of the volume to surface area ratio, since ^{234}Th is mostly surface bound whereas C is distributed evenly throughout the particle [see review by *Buesseler et al*., 2006]. However, the relation between PC/^{234}Th ratio and particle size is not straight forward, and the magnitude of this change further depends on whether larger particles are composed of aggregated smaller particles and whether that aggregation occurred via physical or biologically mediated processes (i.e., grazing and fecal pellet production). In fact, in our study, smaller particles have consistently higher PC/^{234}Th ratios than larger particles, by an average factor of 2.0 ± 0.9 ($p < 0.0001$; $n = 80$). Relatively higher PC/^{234}Th ratios in small particles have been reported previously by other studies in other regions [*Buesseler et al*., 1995; *Bacon et al*., 1996, Equatorial Pacific; *Santschi et al*., 2003; *Hung et al*., 2004, 2010, Gulf of Mexico; *Cai et al*., 2006; *Hung and Gong*, 2007, China Sea and Kuroshio Current; *Jacquet et al*., 2011; *Planchon et al*., 2013, Southern Ocean]. As shown earlier, PC/^{234}Th ratios from both, small and large particles, measured in ISP particles significantly decrease with depth, a trend consistent with a number of prior studies, likely due to (i) a reduction in biological production with increasing depth, (ii) preferential loss of C (and N) relative to ^{234}Th, (iii) potential changes in surface binding

ligands with depth, and/or (iv) increasing particulate ^{234}Th activities due to scavenging [*Rutgers van der Loeff et al*., 2002; *Buesseler et al*., 2006].

Settling speeds may reduce the PC/^{234}Th ratios measured in particles that reach deeper waters since faster sinking particles may be less influenced by biotic and abiotic processes due to their shorter residence times in the water column. Sinking velocities at 100 m were estimated by dividing the ^{234}Th flux at 100 m by the ^{234}Th concentration of the sinking particles collected at that same depth [*Bacon et al*., 1996]. Since ^{234}Th activities were measured in both the small and large ISP particles, we estimated sinking velocities by assuming that the ^{234}Th removal was due to a combination of both small and large particles, or due to large particles alone, thus providing a range of sinking velocities. The average settling velocity determined using integrated WC fluxes and both size classes combined was 5 ± 2 m d^{-1}, while that for the large particles was 23 ± 7 m d^{-1}. When using ^{234}Th fluxes determined directly from ST samples, average sinking velocities increased by a factor of 2 (9 ± 5 m d^{-1} for combined size classes and 47 ± 24 m d^{-1} for large particles).

Based on Stokes' Law, a particle has to be either large or dense enough to overcome the friction force associated with the viscosity of the fluid in order to sink through the water column. One would therefore expect, for the same particle density, that the larger the particle, the faster it would sink, thereby reducing the time period the particle was subjected to breakdown within the water column. Hence, if residence time plays a role in setting the PC/^{234}Th ratio, one would expect a more rapid decrease in PC/^{234}Th ratios in smaller particles with depth (faster attenuation rates) than in larger particles, as a first approximation and assuming no subsurface production of small particles. In order to investigate this prospect further, we calculated an attenuation rate of the PC(PN)/^{234}Th ratio using a power law function in analogy to the classic *Martin et al*. [1987] formulation for carbon flux to depth, where the size of the *b* term indicates the rate of PC/^{234}Th attenuation [equation (2)]. In this formulation, the general rate of change in the element/^{234}Th ratio is a combination of the net change in ^{234}Th particle activities due to adsorption, desorption, and remineralization, and a decrease in the PC and PN content due to remineralization (Figure 5). In this data set, PC and PN concentrations decreased rapidly with depth relative to the small and inconsistent observed increases in specific particulate ^{234}Th activities. Therefore, attenuation of PC and PN is the dominant influence on the *b* term (Table S1). The higher *b* exponents for PN compared to PC are consistent with the more labile nature of N [*Gordon*, 1971]. Additionally, results suggest that PC and PN (relative to ^{234}Th) are attenuated at a similar or faster rate in small versus large ISP particles (Figure 5). Hence, these results support the hypothesis that residence time plays a role in setting the PC and PN to ^{234}Th ratio recorded in small and large particles with depth and helps to explain the convergence of these ratios deeper in the water column.

Higher elemental/^{234}Th ratios observed in the ST samples implies preferential collection of more rapidly sinking particles with shorter water column residence times. *Rutgers van der Loeff et al*. [2002] proposed that higher PC/^{234}Th ratios in ST material might be due to the collection of fresh aggregates, with particle ratios derived from a surface layer that were minimally altered en route to deeper ST. This explanation is consistent with the similarity observed between the elemental/^{234}Th ratios collected with the ISP from the surface waters and those measured in ST deployed at 100 m in this study. The existence of extra-large particles, with high sinking rates, could also be responsible for the higher PC/^{234}Th ratios obtained in the ST, since these particles are likely generated at the surface and do not appear to be composed of smaller particles given their high PC/^{234}Th (over two orders of magnitude higher than particle aggregates) [e.g., *Luo*, 2013]. However, we have no evidence to validate the existence of such particles in this system.

The more rapid attenuation of PC in small particles versus large particles was also confirmed by examining absolute PC changes with depth (Table S1), using the approach of *Lam et al*. [2011] [equation (3)]:

$$[\mathrm{C}] = [\mathrm{C_o}] \cdot (Z/Z_\mathrm{o})^{-\mathrm{b}} \tag{3}$$

where $[\mathrm{C_o}]$ is the carbon concentration (μmol L^{-1}) at the euphotic zone obtained from the curve fitting, Z is the depth at which we calculate the carbon concentration [C], and Z_o is the depth of the euphotic zone [*Lam and Bishop*, 2007].

A faster attenuation of large particles would be expected if large particles are composed of labile compounds that are consumed and disaggregated as they sink, adding more refractory particles to the small size fraction along the water column. Conversely, a faster attenuation of small particles would be expected if the small

particles were more labile. Using organic biomarkers of particles in different size fractions, *Wakeham and Canuel* [1988] found more labile material in the small size fraction, which they proposed was derived from the disaggregation of marine snow aggregates of fresh and delicate algal material that was not collected in the large size fraction or in sediment traps. They hypothesized that the marine snow contributed disproportionately to disaggregation in their system. Marine snow was qualitatively observed in our ST samples as well [see *White et al*., 2013, Figure 6]. Therefore, differences between small and large particles may also be due to differences in their composition (i.e., source). The fact that PC/PN ratios in larger particles were on average higher than in small particles by a factor of 1.5 ± 0.2 further supports this hypothesis. Larger PC/PN ratios in smaller particles due to preferential remineralization of PN are expected given their longer residence times in the water column. However, in this study, large particles are likely detritus composed of degraded organic matter (lower PC/^{234}Th and PN/^{234}Th ratios than the small particles) poor in nutrients. Indeed, higher δ^{13}C values of large ISP particles suggest that significant degradation of large particles has occurred, presumably through zooplankton grazing and repacking [*Fry and Sherr*, 1984; *Fischer*, 1991]. Similar observations were reported by *Alldredge* [1998], who found that large aggregates were older and more refractory than smaller ones, and by *Alonso-González et al*. [2010], whose organic biomarkers analyses revealed that slow sinking particles had the same degradation state or were fresher than rapidly sinking particles. *Mayor et al*. [2014] recently argued that detritivorous metazoans fragment large particles in order to stimulate "microbial gardening" as a pathway to obtain small particles with labile compounds and nutritious microbial biomass. Therefore, higher PN content in small particles, coupled with the differences observed in δ^{13}C values, suggests that other processes, e.g., particle aggregation and microbial colonization, play a role in the observed differences in the particle size composition observed here.

4.2.3. Terms and Phytoplankton Groups

A global compilation of particle attenuation rates by *Lam et al*. [2011] found that the majority of study areas analyzed (~80%; $n = 55$) were characterized by faster attenuation rates (larger *b* term) for the >53 μm particles relative to the 1–53 μm size class. Is it possible that the Gulf of California and the ETNP are uniquely different than most other studied regions of the global ocean? We compiled PC/^{234}Th data presented in previous studies, including the Equatorial Pacific, Sargasso Sea, China Sea, Gulf of Mexico, Mediterranean Sea, Baltic Sea and Nord Sea fjords, and also the Southern Ocean, and found that PC/^{234}Th ratios do not increase with increasing particle size when pico- and nanoplankton (usually *Synechococcus* and *Prochlorococcus*) dominate the planktonic community. Rather, they either have the opposite trend (PC/^{234}Th ratios decrease with increasing particle size) [*Buesseler et al*., 1995; *Guo et al*., 2002; *Santschi et al*., 2003; *Hung et al*., 2004, 2010; *Cai et al*., 2006; *Hung and Gong*, 2007; *Jacquet et al*., 2011; *Planchon et al*., 2013] or there is no clear pattern between particle size and PC/^{234}Th ratio [*Speicher et al*., 2006; *Brew et al*., 2009; *Lepore et al*., 2009; *Hung and Gong*, 2010; *Stewart et al*., 2010]. Furthermore, when particles were collected according to their settling velocities in regions dominated by small cells, higher PC/^{234}Th ratios were found in slow sinking compared to fast sinking particles [*Gustafsson et al*., 2006], or there was no clear trend [*Szlosek et al*., 2009]. Using published data from the studies mentioned above, we calculated *b* terms (when possible) for small and large particles and compared them with the global compilation of data presented in *Lam et al*. [2011] (Figure 7). We then took the ratio of the *b* term for large and small particles (LP/SP *b* ratio) such that a ratio of 1 indicates similar attenuation rates, a ratio higher than 1 suggests faster attenuation of large particles, and a ratio less than 1 suggests faster attenuation of small particles. Although the data are variable, LP/SP *b* ratios are ≤ 1 in 60% of the stations dominated by picoplankton, compared to 50% and 30% for nanoplankton- and microplankton-dominated stations. This finding suggests that globally, small particles are attenuated at a similar or faster rate than large particles in regions with pico- and nanoplankton dominance. There were several stations where data are available that appear to be in the midst of transitioning from food webs dominated by small phytoplankton to those dominated by larger taxa, particularly diatoms. When all data are combined, comparisons between the same stations sampled during different seasons show that, regardless of the dominant group, when the importance of diatoms increases, values for the LP/SP *b* ratio become higher, mainly due to the increase in the *b* term of the large particles. These results indicate the importance of phytoplankton community in the attenuation rates of sinking particles and continue to support arguments against using "global" or "ocean basin" *b* terms in modeling efforts to estimate C export to the deep sea.

4.2.4. Small Particles and Export Fluxes

The discussion above demonstrates how the element/^{234}Th ratio may change with both depth and region depending on the sampling method, particle size, and food web structure. Historically, larger particles have been assumed to dominate particle export [*Michaels and Silver*, 1988], such that the larger size fractions of ISP

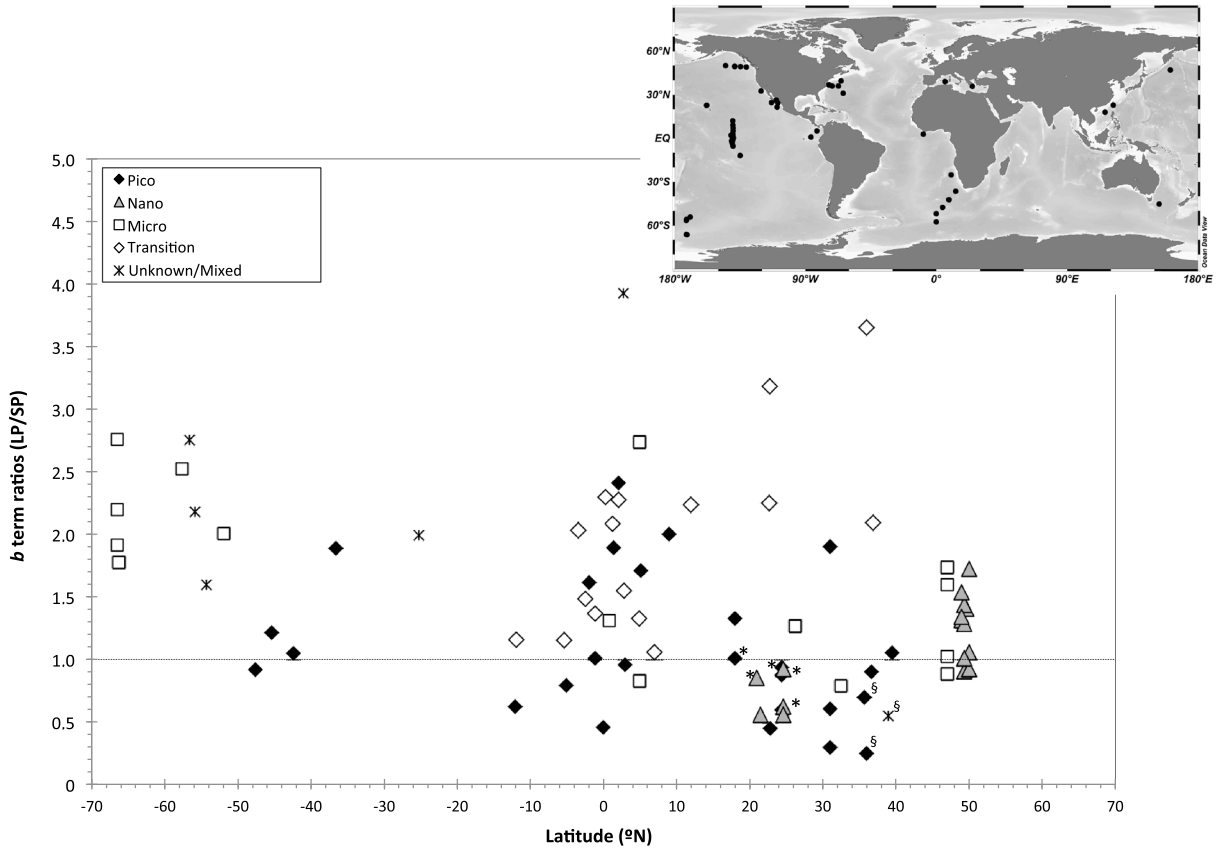

Figure 7. Global compilation of attenuation rate (*b* terms) ratios of large particles (>53 μm) versus small particles (1–53 μm) collected with ISPs including this study. The *b* terms have been obtained applying the power law fit from equation (3) to PC except for those stations marked with *, which have been obtained using the fit to PC/^{234}Th following equation (2). The *b* terms used at those stations marked with § were also obtained using fits to PC/^{234}Th following equation (2), but the small particle fraction only considered particles between 10–20 μm. The horizontal grey line indicates the 1:1 relationship between the *b* terms of large and small particles, indicating that both particle sizes are attenuated at the same rate. Different symbols indicate the dominant particle size at the study site reported by the authors or derived from other studies conducted in the same region during the same season. Due to lack of detail regarding particle size abundances and distribution, when referring to "small particles" and "large particles", the data have been grouped as "pico" and "micro", respectively. The stations dominated by "nano" were clearly defined as such in the original studies. For the majority of studies, however, pico- and nano-dominated stations were usually not differentiated. Therefore, stations considered as pico-dominated might include areas where nanoplankton was also important. The "transition" stations are those that appeared to be transitioning from food webs dominated by small phytoplankton to those dominated by larger taxa, regardless of the dominant group at the sampling time. Map inset shows the locations of data from *Cai et al*. [2006], *Hung and Gong* [2007], *Lepore et al*. [2009], *Stewart et al*. [2010], *Jacquet et al*. [2011], *Planchon et al*. [2013], and the studies included in *Lam et al*. [2011], *Bishop et al*. [1977,1978, 1980, 1986], *Bishop and Fleisher* [1987], *Bishop* [1992, 1999], *Bishop et al*. [1999], *Lam and Bishop* [2007], and *Bishop and Wood* [2008].

(>53 μm) and ST particles are used to convert ^{234}Th fluxes into elemental export [*Buesseler et al*., 2006]. More recent studies have challenged this view. *Richardson and Jackson* [2007] used inverse modeling approaches to argue that pico- and nanoplankton can contribute to carbon export at rates proportional to their production, particularly in oligotrophic regions. Although this approach has been questioned by *Landry et al*. [2011], field studies by *Brew et al*. [2009], *Lomas and Moran* [2011], and *Alonso-González et al*. [2010] in the oligotrophic subtropics using organic biomarkers and degradation pigments estimate that smaller particles contribute as much as 50% of the measured POC export fluxes. *Dunne et al*. [1997] argued that in the Equatorial Pacific, the >53 μm ISP particles did not represent the sinking material that reached the ST. *Grob et al*. [2007] and *Hung and Gong* [2010] also suggested that the contribution of particles <50 μm to the settling flux could be larger than previously thought, and more recently, *Hung et al*. [2012] reported scanning electron microscopy images showing that the bulk of sinking particles contained mostly particles of such size. DNA analysis from trap material has further shown that small-sized eukaryotic taxa and cyanobacteria can contribute to the sinking particle flux below the euphotic zone [*Amacher et al*., 2013]. Using gel traps, *Durkin et al*. [2015] have also provided evidence of the importance of small particle sizes to carbon export flux in the upper mesopelagic

waters. Signs of small particles sinking were also reported by *Xu et al.* [2011] who found the best agreement of POC/^{234}Th ratios with those in ST for intermediate-sized (10–50 μm) rather than larger (>50 μm) particles, suggesting that these smaller particles dominated the export flux. In that same study, the dominance of nanoplankton and pico-prymnesiophytes was proposed as the source of disagreement between POC/^{234}Th in large (>50 μm) ISP particles and ST particles.

Our results are consistent with the new paradigm that small particles play a significant role in particle settling fluxes, especially in oligotrophic regions. Based on HPLC analyses, the phytoplankton community was dominated by picophytoplankton, especially in the GC interior and Transition zone (GC4-1, in the upper 30 m, GC4-2, GC4-8, and GC4-9) [*White et al.*, 2013], with picophytoplankton abundances decreasing and nanophytoplankton abundances increasing when exiting the gulf toward the northern stations. Higher abundances of microphytoplankton were found at all the stations between 30 and 50 m, especially at GC4-1 and GC4-12, where diatoms dominated [*White et al.*, 2013]. Particle size distribution (PSD) analysis (living and detrital particles) confirms these trends (Figure 4): PSD profiles showed a clear shift from small particles toward larger particles while moving out of GC and north along the ETNP transect.

A better agreement was found between measured fluxes derived using ST and ISP small particle ratios (Figure 6), due to their more similar elemental/^{234}Th ratios. To further explore the composition of the particulate samples, C and N isotopic composition (Table S1) was examined. These data provide insight into particle sources and remineralization. For example, the δ^{13}C values of particles can indicate terrestrial (>−24‰) versus marine sources (−22‰ to −10‰) [*Peterson and Fry*, 1987], when combined with particulate C/N ratios (marine ~6–7; terrestrial >20) [*Hedges et al.*, 1986]. We found a significant difference between the δ^{13}C values of large ISP particles and ST particles ($p < 0.0001$; $n = 58$), while there was no difference between δ^{13}C values in small ISP particles versus ST particles ($p > 0.5$; $n = 58$). Lower PN concentrations and higher δ^{13}C values of larger ISP particles are consistent with enhanced degradation as well as zooplankton grazing and repackaging [*Fry and Sherr*, 1984] (e.g., fecal pellets). The reduced degradation signal observed in the smaller size class suggests that such particles settle through the water column and into the ST in the form of large aggregates [*Lomas and Moran*, 2011].

Aggregation is enhanced by TEP, which form the mucus matrix of most marine snow [*Passow*, 2002; *Engel et al.*, 2004; *Verdugo et al.*, 2004]. *Guo et al.* [2002] argued that small particles (<10 μm) may coagulate into the larger particle size class (10–53 μm) on timescales of <1 day. This rapid aggregation, and subsequent faster sinking, would also explain how small relatively undegraded particles reached the ST, leading to an increase in export flux efficiency in this region during the summer months. While marine snow aggregation dynamics remain enigmatic [*Boyd and Trull*, 2007], qualitative observations of the ST material suggest that in our study area, small particle sinking is driven by aggregation into marine snow and through zooplankton-mediated packaging of small particles in fecal pellets, which are rarely captured by large particle ISP measurements using certain types of filter holders that are not designed specifically to retain these particles [*Trent et al.*, 1978; *Gardner et al.*, 2003; *Bishop et al.*, 2012].

Data obtained at station GC4-2, which was sampled twice, 6 days apart, for particles also support our assertion that small particles are settling into the ST. During its second occupation, there was an increase in the PC/^{234}Th ratio in ST particles (5.5 to 8.6) and the maximum for PC/^{234}Th ratios of small ISP particles moved deeper in the water column, while the distribution of PC/^{234}Th ratio for large ISP particles remained unchanged. The PC/^{234}Th ratio from the ST material collected during the reoccupation (8.6) matched the ratio of the small particles collected with the ISP at 20 m during the first occupation (8.9). The settling speed for small particles derived using this observation is ~13 m d^{-1} (e.g., 80 m in 6 days), in agreement with the lower range of sinking velocities estimated earlier (see section 4.2.2). This "delay" was not observed in the PC/^{234}Th ratios of large particles: They were 6.4 and 8.6 at 20 m for GC4-2 and GC4-2b, respectively, agreeing with the ST ratios measured at each time point and suggesting a much faster settling speed (in the upper range of the speeds estimated in section 4.2.2) for this particle size.

4.3. Particle Fluxes and Export Efficiency

Within the GC, previous studies have shown that seasonal changes in phytoplankton community structure influence bSi and carbonate fluxes to depth, whereas PC and PN remain constant throughout the year [*Thunell*, 1998; *Lyons et al.*, 2011]. Typically, high bSi fluxes occur from late fall to early spring in response

to upwelling-driven diatom blooms. Increasing stratification during the summer decreases primary production, and carbonate becomes the main source of the biomineral sediment flux [*Thunell*, 1998; *Lyons et al*., 2011]. Our results showed minimal PIC concentrations in the particulate samples collected (either by ISP or ST), likely due to the timing of our sampling. In agreement with *Thunell* [1998], we did not observe significant fluxes of bSi (Figure 6 and Table 2), except at stations GC4-1 and GC4-12, the ones with highest NPP (Table 1) and where pigment analysis and microscopy observations provided evidence of a diatom-dominant phytoplankton community structure below 30 m and within the upper 60 m, respectively. In general, higher PC and PN fluxes occurred where picophytoplankton and diazotrophs were more abundant (GC4-2, GC4-8, and GC4-11) or where a diatom-dominated phytoplankton community was observed (GC4-1 and GC4-12).

To estimate the efficiency of export, we calculated *ThE* ratios by dividing the ^{234}Th-derived PC export fluxes at 100 m by NPP rates, as defined by *Buesseler* [1998]. In those regions with efficient recycling (i.e., low PC flux below the depth of interest), *ThE* ratios should be relatively low (<10%). On the other hand, *ThE* ratios in excess of 10–50% are typically found not only during high production events but when production and export are decoupled, such as in high latitudes [*Buesseler*, 1998; *Buesseler et al*., 2001; *Schmidt et al*., 2002; *Thomalla et al*., 2006; *Baumann et al*., 2013]. We further determined export efficiencies following that of *Buesseler and Boyd* [2009], where export efficiencies are calculated by normalizing PC fluxes to the depth of the Ez and at a reference depth of 100 m below Ez (~200 m in this area) to allow for a comparison across regions with significantly different light penetration depths, where the major production of particles (that scavenge ^{234}Th) takes place. Thus, the normalized export efficiencies obtained are a combination of two terms: (i) the export flux down to the base of the Ez relative to NPP and (ii) the flux attenuation down to an "attenuation depth", 100 m below the Ez. The terms T_{100} and Ez ratio presented in Table 2 refer to the PC flux at the attenuation depth divided by the PC flux at the Ez and the PC flux at the Ez divided by NPP, respectively. Therefore, T_{100} and Ez ratio provide information regarding the importance of both processes responsible for the calculated export efficiencies; e.g., high export efficiencies could be due to efficient export down to the bottom of the Ez (= high Ez-ratio values) or due to weak attenuation [= low T_{100} values or low "b" terms from equations (2) and (3)] (Table 2).

All the estimates of *ThE* ratios, based on ST and WC fluxes, are presented in Table 2 and Figure 8, where similar trends between the different approaches can be observed. PC-normalized export efficiencies are also presented in Table 2, to be consistent with the literature. The results indicate that at stations GC4-1 and GC4-12, where diatoms were the dominant phytoplankton and C fixation rates were highest, PC export efficiencies at 100 m were among the lowest measured, regardless of the approach used for derivation (less than 10% using ISP ratios and 18–27% when using ST ratios and fluxes; Table 2), similar to the results reported by *Maiti et al*. [2013] and *Lam and Bishop* [2007] in the Southern Ocean. In contrast, the highest *ThE* ratios occurred at stations with higher abundances of picophytoplankton, GC4-2 and GC4-8, and where qPCR assays also revealed the highest specific planktonic nitrogenase gene (*nifH*) copies and gene expression recorded for large diazotrophs (*Trichodesmium* and *Richelia* symbioses) [*White et al*., 2013]. Export efficiencies along the ETNP transect, where nanoplankton increased in relative abundance, were moderate to low (<40%, using ST material, and <5% using ISP ratios, excluding GC4-11). Station GC4-11 had higher *ThE* ratios (~50–60% using ST material and 9–15% using ISP ratios) than GC4-10 and GC4-12, and was also the station with the highest abundance of *nifH* transcription by unicellular diazotrophic cyanobacteria of the group A (UCYN-A) and where highest N_2 fixation rates were also observed [*White et al*., 2013].

White et al. [2013] reported absolute C fixation rates measured in the euphotic zone and the PC export efficiency recorded by ST in the study area during summer and winter months of 2005. Despite the differences in C fixation, export efficiencies in summer were equivalent or higher than winter records (average export efficiency of 34% and 18%, for summer and winter, respectively). The results presented here also show evidence of a high PC export efficiency during the summer of 2008. Therefore, our results support the hypothesis of more efficient particle export during the summer as a major reason for the lack of seasonality observed in carbon and nutrient fluxes in deep moored ST in the GC [*Thunell*, 1998; *Lyons et al*., 2011]. The fact that most stations, with the exception of GC4-1 and GC4-12, were dominated by small phytoplankton further supports the supposition that pico- and nanophytoplankton and associated aggregation processes play an important role in driving PC fluxes in oligotrophic regions globally.

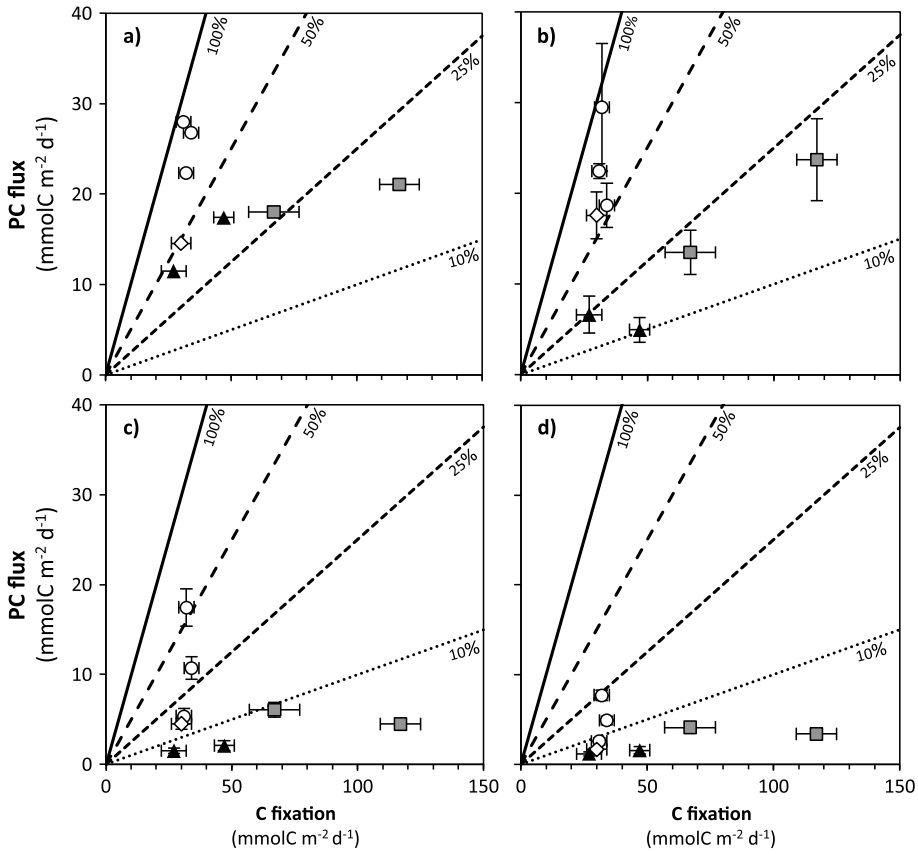

Figure 8. *ThE* ratios resulting from the various methods used to estimate PC fluxes. Symbols indicate high relative abundance of large diazotroph (open circles), small diazotroph (white diamonds), and diatoms (grey squares). Black triangles are stations were neither diatoms nor diazotrophs were abundant. Diagonal lines represent 10%, 25%, 50%, and 100% *ThE*. (a) PC flux is directly obtained from ST, (b) PC flux is derived from water column ^{234}Th fluxes and ST ratios, (c) Water column-derived ^{234}Th fluxes and small particle ratios, and (d) water column-derived ^{234}Th fluxes and large particle ratios.

5. Conclusions

We used ^{234}Th as a tracer to estimate particle fluxes in a region where previous studies have suggested that particle export is more efficient during lower productivity summer months as a result of a change in food web dynamics, e.g., from larger to smaller plankton. PC and PN data were obtained from free-drifting surface-tethered sediment traps and large-volume in situ pumps in order to compare methodologies and to provide more detailed profiles of elemental/^{234}Th ratios over the upper 500 m in two different particle size classes (1–53 μm and >53 μm). Large variability in values of PC and PN to ^{234}Th ratios was observed in the surface layer, with ratios for both size classes decreasing with depth. Although small particles had higher elemental to ^{234}Th ratios at the surface, attenuation rates were significantly higher for the smaller size class, allowing both size class ratios to converge to 1–5 μmol dpm^{-1} by 100 m. Elemental/^{234}Th ratios measured in sediment trap materials collected at 100 m tended to be higher than those measured at the same depth using in situ pumps but agreed with in situ pumps ratios obtained from surface waters. This implies that sediment traps may have been more efficient in collecting rapidly sinking aggregated particles from surface waters that were less affected by decomposition processes. Elemental/^{234}Th ratios in small particles collected at 100 m were in better agreement with sediment trap ratios than those of large particles, suggesting a significant contribution of small particles to the export flux, even though small particle attenuation rates exceeded those of the larger size class. Particle size distribution measurements confirmed high abundances of small particles in the study area, especially within the GC. Supporting elemental data include the strong agreement between higher PN concentrations and lower δ^{13}C values in small particles with sediment trap material.

PC and PN fluxes were variable, but higher export fluxes did not always correspond to higher export efficiencies, reflecting the variability of the phytoplankton community structure observed across the region. Stations dominated by diatoms and with the highest C fixation measurements were among the lowest in export efficiency. In contrast, stations dominated by picophytoplankton had the highest export efficiencies. The presence of diazotrophs also favored enhanced export efficiency, although since observed N_2 fixation rates were highly variable, diazotrophic activity alone cannot explain the observed patterns of C export efficiency [*White et al.*, 2013].

Combined, we argue that small phytoplankton are important contributors to particle export during the summer (oligotrophic period) in the GC and ETNP region. Comparison of our results with previous work suggests that faster attenuation rates in small particles with depth are a ubiquitous feature of the world's oligotrophic oceans when smaller phytoplankton taxa dominate the food web. In this study, despite the observed higher attenuation rates of small particles, stations dominated by small phytoplankton are characterized by more efficient export. As a result, export efficiencies are higher where smaller particles dominate the flux and may help to explain the apparent lack in correlation between PC export rates with NPP in oligotrophic regions [*Burd et al.*, 2010].

Our results argue for the multiple particle size class sampling when using the ^{238}U:^{234}Th disequilibrium technique to determine export rates and the continued use of multiple methods to quantify PC export to depth. Such knowledge is critical for better predicting biological responses to large-scale changes in climate that are already influencing the marine system. It will require a regional and ecosystem specific approach, with special attention paid to small plankton, which historically have been neglected as an efficient pathway for carbon export. Further work to understand the characteristics of material collected with sediment traps and in situ pumps over seasonal timescales will provide much needed information regarding the mechanisms, origin, and abundances of the particles that reach deeper layers, enhancing our understanding of particle dynamics in this region and other oligotrophic systems.

Acknowledgments
Elemental composition for particulate samples is available in Table A.1. Funding for this project was provided by NSF OCE-0726290 (C.B.N.), EU FP7-MC-IIF-220485 (C.B.N. and P.M.), MEC CTM2007-31241-E/MAR (P.M.), the ICREA Academia (P.M.) and MERS (2014 SGR – 1356) (P.M. and V.P.), funded by the Generalitat de Catalunya, Ph.D. Fellowships from Spain's Ministerio de Educación y Ciencia through grants AP-2009-4733 (V.P.) and BES-2004-3348 (E.V.), NSF OCF-0962362 (A.W.), NASA New Investigator Award NNX10AQ81G (A.W.), Sloan Research Fellowship (A.W.), NSF OCE-0726543 (B.N.P.), and NSF OCE-0726422 (F.P.). We would like to thank the captain and the crew of the R/V *New Horizon* and the scientists on board for their cooperation and assistance during the cruise. We wish also to acknowledge Natalie Wallsgrove and Wendy Plessinger for sample analysis, Maxi Castrillejo and Valentí Rodellas for providing helpful comments on an early draft, and Dieter Wolf-Gladrow for statistical support. This is SOEST contribution number 9483.

References

Alldredge, A. (1998), The carbon, nitrogen and mass content of marine snow as a function of aggregate size, *Deep Sea Res., Part I*, *45*(4), 529–541.

Alonso-González, I. J., J. Arístegui, C. Lee, A. Sanchez-Vidal, A. Calafat, J. Fabrés, P. Sangrá, P. Masqué, A. Hernández-Guerra, and V. Benítez-Barrios (2010), Role of slowly settling particles in the ocean carbon cycle, *Geophys. Res. Lett.*, *37*, L13608, doi:10.1029/2010GL043827.

Altabet, M. A., C. Pilskaln, R. Thunell, C. Pride, D. Sigman, F. Chavez, and R. Francois (1999), The nitrogen isotope biogeochemistry of sinking particles from the margin of the Eastern North Pacific, *Deep Sea Res., Part I*, *46*(4), 655–679.

Amacher, J., S. Neuer, and M. Lomas (2013), DNA-based molecular fingerprinting of eukaryotic protists and cyanobacteria contributing to sinking particle flux at the Bermuda Atlantic time-series study, *Deep Sea Res., Part II*, *93*, 71–83, doi:10.1016/j.dsr2.2013.01.001.

Bacon, M. P., J. K. Cochran, D. Hirschberg, T. R. Hammar, and A. P. Fleer (1996), Export flux of carbon at the equator during the EqPac time-series cruises estimated from ^{234}Th measurements, *Deep Sea Res., Part II*, *43*(4–6), 1133–1153.

Badan-Dangon, A., C. E. Dorman, M. A. Merrifield, and C. D. Winant (1991), The lower atmosphere over the Gulf of California, *J. Geophys. Res. Ocean.*, *96*(C9), 16,877–16,896.

Baumann, M. S., S. B. Moran, M. W. Lomas, R. P. Kelly, and D. W. Bell (2013), Seasonal decoupling of particulate organic carbon export and net primary production in relation to sea-ice at the shelf break of the eastern Bering Sea: Implications for off-shelf carbon export, *J. Geophys. Res. Ocean.*, *118*, 5504–5522, doi:10.1002/jgrc.20366.

Beaugrand, G., M. Edwards, K. Brander, C. Luczak, and F. Ibanez (2008), Causes and projections of abrupt climate-driven ecosystem shifts in the North Atlantic, *Ecol. Lett.*, *11*(11), 1157–1168.

Benitez-Nelson, C., K. O. Buesseler, D. M. Karl, and J. Andrews (2001), A time-series study of particulate matter export in the North Pacific Subtropical Gyre based on ^{234}Th:^{238}U disequilibrium, *Deep Sea Res., Part I*, *48*(12), 2595–2611.

Benitez-Nelson, C. R., and M. Charette (2004), Uncertainty versus variability in upper ocean carbon flux estimates, *Limnol. Oceanogr.*, *49*(4), 1218–1220.

Benitez-Nelson, C. R., and W. S. Moore (2006), Future applications of ^{234}Th in aquatic ecosystems, *Mar. Chem.*, *100*(3), 163–165.

Benitez-Nelson, C. R., R. R. Bidigare, T. D. Dickey, M. R. Landry, C. L. Leonard, S. L. Brown, F. Nencioli, Y. M. Rii, K. Maiti, and J. W. Becker (2007), Mesoscale eddies drive increased silica export in the subtropical Pacific Ocean, *Science*, *316*(5827), 1017–1021.

Bishop, J. K. B. (1992), POC from MULVFS casts, 25 September 2002, JGOFS Data Server, U.S. JGOFS Data Manag. Off. WHOI, Woods Hole, Mass. [Available at http://usjgofs.whoi.edu/jg/serv/jgofs/eqpac/ tt007/mulvfs_POC.html0 (Accessed 6 February 2010).]

Bishop, J. K. B. (1999), Transmissometer measurement of POC, *Deep Sea Res., Part I*, *46*(2), 353–369.

Bishop, J. K. B., and M. Q. Fleisher (1987), Particulate manganese dynamics in Gulf Stream warm-core rings and surrounding waters of the N.W. Atlantic, *Geochim. Cosmochim. Acta*, *51*(10), 2807–2825, doi:10.1016/0016-7037(87)90160-8.

Bishop, J. K. B., and T. J. Wood (2008), Particulate matter chemistry and dynamics in the twilight zone at VERTIGO, ALOHA and K2 sites, *Deep Sea Res., Part I*, *55*(12), 1684–1706, doi:10.1016/j.dsr.2008.07.012.

Bishop, J. K. B., J. M. Edmond, D. R. Ketten, M. P. Bacon, and W. B. Silker (1977), The chemistry, biology, and vertical flux of particulate matter from the upper 400 m of the equatorial Atlantic Ocean, *Deep Sea Res.*, *24*(6), 511–548.

Bishop, J. K. B., R. W. Collier, D. R. Kettens, and J. M. Edmond (1980), The chemistry, biology, and vertical flux of particulate matter from the upper 1500 m of the Panama Basin, *Deep Sea Res., Part A*, *27*(8), 615–640, doi:10.1016/0198-0149(80)90077-1.

Bishop, J. K. B., J. C. Stepien, and P. H. Wiebe (1986), Particulate matter distributions, chemistry and flux in the Panama Basin: Response to environment forcing, *Prog. Oceanogr.*, *17*(1–2), 1–59, doi:10.1016/0079-6611(86)90024-8.

Bishop, J. K. B., S. E. Calvert, and M. Y. S. Soon (1999), Spatial and temporal variability of {POC} in the northeast Subarctic Pacific, *Deep Sea Res., Part II*, *46*(11–12), 2699–2733, doi:10.1016/S0967-0645(99)00081-8.

Bishop, J. K. B., P. J. Lam, and T. J. Wood (2012), Getting good particles: Accurate sampling of particles by large volume in-situ filtration, *Limnol. Oceanogr. Methods*, *10*, 681–710, doi:10.4319/lom.2012.10.681.

Bopp, L., O. Aumont, P. Cadule, S. Alvain, and M. Gehlen (2005), Response of diatoms distribution to global warming and potential implications: A global model study, *Geophys. Res. Lett.*, *32*, L19606, doi:10.1029/2005GL023653.

Boyd, P. W., and T. W. Trull (2007), Understanding the export of biogenic particles in oceanic waters: Is there consensus?, *Prog. Oceanogr.*, *72*(4), 276–312, doi:10.1016/j.pocean.2006.10.007.

Brand, L. E. (1994), Physiological ecology of marine coccolithophores, in *Coccolithophores*, pp. 39–49, Cambridge Univ. Press, Cambridge, U. K.

Bray, N. A., and J. M. Robles (1991), Physical oceanography of the Gulf of California, in *Gulf Penins. Prov. California*, vol. 31, edited by J. P. Dauphin and B. R. T. Simoneit, pp. 1122–1131, Am. Assoc. Petrol. Geol., Tulsa, Okla.

Brew, H. S., S. B. Moran, M. W. Lomas, and A. B. Burd (2009), Plankton community composition, organic carbon and thorium-234 particle size distributions, and particle export in the Sargasso Sea, *J. Mar. Res.*, *67*(6), 845–868.

Bricaud, A., A. Morel, M. Babin, K. Allali, and H. Claustre (1998), Variations of light absorption by suspended particles with chlorophyll a concentration in oceanic (case 1) waters: Analysis and implications for bio-optical models, *J. Geophys. Res.*, *103*(C13), 31,033–31,044, doi:10.1029/98JC02712.

Buesseler, K., L. Ball, J. Andrews, C. Benitez-Nelson, R. Belastock, F. Chai, and Y. Chao (1998), Upper ocean export of particulate organic carbon in the Arabian Sea derived from thorium-234, *Deep Sea Res., Part II*, *45*(10–11), 2461–2487.

Buesseler, K. O. (1991), Do upper-ocean sediment traps provide an accurate record of particle flux?, *Nature*, *353*(6343), 420–423.

Buesseler, K. O. (1998), The decoupling of production and particulate export in the surface ocean, *Global Biogeochem. Cycles*, *12*(2), 297–310, doi:10.1029/97GB03366.

Buesseler, K. O., and P. W. Boyd (2009), Shedding light on processes that control particle export and flux attenuation in the twilight zone of the open ocean, *Limnol. Oceanogr.*, *54*(4), 1210–1232.

Buesseler, K. O., M. P. Bacon, J. Kirk Cochran, and H. D. Livingston (1992), Carbon and nitrogen export during the JGOFS North Atlantic Bloom Experiment estimated from ^{234}Th:^{238}U disequilibria, *Deep Sea Res., Part A*, *39*(7–8), 1115–1137.

Buesseler, K. O., A. F. Michaels, D. A. Siegel, and A. H. Knap (1994), A three dimensional time-dependent approach to calibrating sediment trap fluxes, *Global Biogeochem. Cycles*, *8*(2), 179–193, doi:10.1029/94GB00207.

Buesseler, K. O., J. A. Andrews, M. C. Hartman, R. Belastock, and F. Chai (1995), Regional estimates of the export flux of particulate organic carbon derived from thorium-234 during the JGOFS EqPac program, *Deep Sea Res., Part II*, *42*(2–3), 777–791.

Buesseler, K. O., L. Ball, J. Andrews, J. K. Cochran, D. J. Hirschberg, M. P. Bacon, A. Fleer, and M. Brzezinski (2001), Upper ocean export of particulate organic carbon and biogenic silica in the Southern Ocean along 170 W, *Deep Sea Res., Part II*, *48*(19–20), 4275–4297.

Buesseler, K. O., C. R. Benitez-Nelson, S. B. Moran, A. Burd, M. Charette, J. K. Cochran, L. Coppola, N. S. Fisher, S. W. Fowler, and W. D. Gardner (2006), An assessment of particulate organic carbon to thorium-234 ratios in the ocean and their impact on the application of ^{234}Th as a POC flux proxy, *Mar. Chem.*, *100*(3–4), 213–233.

Buesseler, K. O., A. N. Antia, M. Chen, S. W. Fowler, W. D. Gardner, O. Gustafsson, K. Harada, A. F. Michaels, M. R. van der Loeff, and M. Sarin (2007), An assessment of the use of sediment traps for estimating upper ocean particle fluxes, *J. Mar. Res.*, *65*, 345–416.

Buesseler, K. O., C. Lamborg, P. Cai, R. Escoube, R. Johnson, S. Pike, P. Masqué, D. McGillicuddy, and E. Verdeny (2008), Particle fluxes associated with mesoscale eddies in the Sargasso Sea, *Deep Sea Res., Part II*, *55*(10–13), 1426–1444.

Burd, A. B., G. A. Jackson, and S. B. Moran (2007), The role of the particle size spectrum in estimating POC fluxes from disequilibrium, *Deep Sea Res., Part I*, *54*(6), 897–918.

Burd, A. B., D. Hansell, D. Steinberg, T. Anderson, J. Arístegui, F. Balta, S. Beaupré, K. Buesseler, F. DeHairs, and G. Jackson (2010), Assessing the apparent imbalance between geochemical and biochemical indicators of meso- and bathypelagic biological activity: What the @$#! is wrong with present calculations of carbon budgets?, *Deep Sea Res., Part II*, *57*(16), 1557–1571, doi:10.1016/j.dsr2.2010.02.022.

Cai, P., M. Dai, W. Chen, T. Tang, and K. Zhou (2006), On the importance of the decay of ^{234}Th in determining size-fractionated C/^{234}Th ratio on marine particles, *Geophys. Res. Lett.*, *33*, L23602, doi:10.1029/2006GL027792.

Castro, C. G., F. P. Chavez, and C. A. Collins (2001), Role of the California Undercurrent in the export of denitrified waters from the eastern tropical North Pacific, *Global Biogeochem. Cycles*, *15*(4), 819–830, doi:10.1029/2000GB001324.

Castro, R., R. Durazo, A. Mascarenhas, C. A. Collins, and A. Trasviña (2006), Thermohaline variability and geostrophic circulation in the southern portion of the Gulf of California, *Deep Sea Res., Part I*, *53*(1), 188–200.

Chen, J. H., R. Lawrence Edwards, and G. J. Wasserburg (1986), ^{238}U, ^{234}U and ^{232}Th in seawater, *Earth Planet. Sci. Lett.*, *80*, 241–251.

Cline, J. D., and F. A. Richards (1972), Oxygen deficient conditions and nitrate reduction in the eastern tropical North Pacific Ocean, *Limnol. Oceanogr.*, *17*, 885–900.

Coale, K. H. (1990), Labyrinth of doom: A device to minimize the "swimmer" component in sediment trap collections, *Limnol. Oceanogr.*, *35*, 1376–1381.

Coale, K. H., and K. W. Bruland (1985), ^{234}Th:^{238}U disequilibria within the California Current, *Limnol. Oceanogr.*, *30*, 22–33.

Cochran, J. K., and P. Masqué (2003), Short-lived U/Th series radionuclides in the ocean: Tracers for scavenging rates, export fluxes and particle dynamics, *Rev. Mineral. Geochem.*, *52*(1), 461–492.

Codispoti, L. A., and F. A. Richards (1976), An analysis of the horizontal regime of denitrification in the eastern tropical North Pacific, *Limnol. Oceanogr.*, *21*(3), 379–388.

DeMaster, D. J. (1991), Measuring biogenic silica in marine sediments and suspended matter, *Geophys. Monogr. Ser.*, *63*, 363–367.

DeVries, T., and C. Deutsch (2014), Large-scale variations in the stoichiometry of marine organic matter respiration, *Nat. Geosci.*, *7*(12), 890–894.

Doney, S. C. (2006), Plankton in a warmer world, *Nature*, *444*, 695–696.

Doney, S. C., M. Ruckelshaus, J. E. Duffy, J. P. Barry, F. Chan, C. A. English, H. M. Galindo, J. M. Grebmeier, A. B. Hollowed, and N. Knowlton (2012), Climate change impacts on marine ecosystems, *Mar. Sci.*, *4*, 11–37.

Dore, J. E., J. R. Brum, L. M. Tupas, and D. M. Karl (2002), Seasonal and interannual variability in sources of nitrogen supporting export in the oligotrophic subtropical North Pacific Ocean, *Limnol. Oceanogr.*, *47*(6), 1595–1607.

Dunne, J. P., J. W. Murray, J. Young, L. S. Balistrieri, and J. Bishop (1997), ^{234}Th and particle cycling in the central equatorial Pacific, *Deep Sea Res., Part II*, *44*(9–10), 2049–2083.

Dunne, J. P., J. W. Murray, A. K. Aufdenkampe, S. Blain, and M. Rodier (1999), Silicon-nitrogen coupling in the equatorial Pacific upwelling zone, *Global Biogeochem. Cycles*, *13*(3), 715–726, doi:10.1029/1999GB900031.

Durkin, C. A., M. L. Estapa, and K. O. Buesseler (2015), Observations of carbon export by small sinking particles in the upper mesopelagic, *Mar. Chem.*, doi:10.1016/j.marchem.2015.02.011.

Duteil, O., and A. Oschlies (2011), Sensitivity of simulated extent and future evolution of marine suboxia to mixing intensity, *Geophys. Res. Lett.*, *38*, L06607, doi:10.1029/2011GL046877.

Engel, A., S. Thoms, U. Riebesell, E. Rochelle-Newall, and I. Zondervan (2004), Polysaccharide aggregation as a potential sink of marine dissolved organic carbon, *Nature*, *428*(6986), 929–932.

Feely, R. A., C. L. Sabine, K. Lee, W. Berelson, J. Kleypas, V. J. Fabry, and F. J. Millero (2004), Impact of anthropogenic CO_2 on the $CaCO_3$ system in the oceans, *Science*, *305*(5682), 362–366.

Fischer, G. (1991), Stable carbon isotope ratios of plankton carbon and sinking organic matter from the Atlantic sector of the Southern Ocean, *Mar. Chem.*, *35*(1–4), 581–596, doi:10.1016/S0304-4203(09)90044-5.

Fry, B., and E. B. Sherr (1984), $\delta^{13}C$ measurements as indicators of carbon flow in marine and freshwater ecosystems, *Contrib. Mar. Sci.*, *27*, 13–47.

Gardner, W. D. (1980), Sediment trap dynamics and calibration: A laboratory evaluation, *J. Mar. Res.*, *38*(1), 17–39.

Gardner, W. D. (2000), *Sediment Trap Sampling in Surface Waters*, Cambridge Univ. Press, Cambridge, U. K.

Gardner, W. D., M. J. Richardson, C. A. Carlson, D. Hansell, and A. V. Mishonov (2003), Determining true particulate organic carbon: Bottles, pumps and methodologies, *Deep Sea Res., Part II*, *50*(3), 655–674.

Gardner, W. D., A. V. Mishonov, and M. J. Richardson (2006), Global POC concentrations from in-situ and satellite data, *Deep Sea Res., Part II*, *53*(5), 718–740.

Gnanadesikan, A., J. P. Dunne, and J. John (2012), Understanding why the volume of suboxic waters does not increase over centuries of global warming in an Earth System Model, *Biogeosciences*, *9*(3), 1159–1172.

Gordon, D. C. (1971), Distribution of particulate organic carbon and nitrogen at an oceanic station in the central Pacific, *Deep Sea Res.*, 8, 1127–1134.

Grob, C., O. Ulloa, H. Claustre, Y. Huot, G. Alarcón, and D. Marie (2007), Contribution of picoplankton to the total particulate organic carbon concentration in the eastern South Pacific, *Biogeosciences*, *4*(5), 837–852.

Guo, L., C. C. Hung, P. H. Santschi, and I. D. Walsh (2002), ^{234}Th scavenging and its relationship to acid polysaccharide abundance in the Gulf of Mexico, *Mar. Chem.*, *78*(2), 103–119.

Gustafsson, Ö., P. Andersson, P. Roos, Z. Kukulska, D. Broman, U. Larsson, S. Hajdu, and J. Ingri (2004), Evaluation of the collection efficiency of upper ocean sub-photic-layer sediment traps: A 24-month in situ calibration in the open Baltic Sea using ^{234}Th, *Limnol. Oceanogr. Methods*, *2*, 62–74.

Gustafsson, Ö., J. Larsson, P. Andersson, and J. Ingri (2006), The POC/^{234}Th ratio of settling particles isolated using split flow-thin cell fractionation (SPLITT), *Mar. Chem.*, *100*(3), 314–322.

Hargrave, B. T., and N. M. Burns (1979), Assessment of sediment trap collection efficiency, *Limnol. Oceanogr.*, *24*(6), 1124–1135.

Hays, G. C., A. J. Richardson, and C. Robinson (2005), Climate change and marine plankton, *Trends Ecol. Evol.*, *20*(6), 337–344.

Hedges, J. I., W. A. Clark, P. D. Quay, J. E. Richey, A. H. Devol, and U. d. M. Santos (1986), Compositions and fluxes of particulate organic material in the Amazon River, *Limnol. Oceanogr.*, *31*(4), 717–738.

Honjo, S., S. J. Manganini, R. A. Krishfield, and R. Francois (2008), Particulate organic carbon fluxes to the ocean interior and factors controlling the biological pump: A synthesis of global sediment trap programs since 1983, *Prog. Oceanogr.*, *76*(3), 217–285.

Hung, C.-C., and G.-C. Gong (2007), Export flux of POC in the main stream of the Kuroshio, *Geophys. Res. Lett.*, *34*, L18606, doi:10.1029/2007GL030236.

Hung, C. C., and G. C. Gong (2010), POC/^{234}Th ratios in particles collected in sediment traps in the northern South China Sea, *Estuarine Coastal Shelf Sci.*, *88*(3), 303–310.

Hung, C. C., L. Guo, K. A. Roberts, and P. H. Santschi (2004), Upper ocean carbon flux determined by the ^{234}Th approach and sediment traps using size-fractionated POC and ^{234}Th data from the Gulf of Mexico, *Geochem. J.*, *38*(6), 601–611.

Hung, C. C., C. Xu, P. H. Santschi, S. J. Zhang, K. A. Schwehr, A. Quigg, L. Guo, G. C. Gong, J. L. Pinckney, and R. A. Long (2010), Comparative evaluation of sediment trap and ^{234}Th-derived POC fluxes from the upper oligotrophic waters of the Gulf of Mexico and the subtropical northwestern Pacific Ocean, *Mar. Chem.*, *121*(1), 132–144.

Hung, C. C., G. C. Gong, and P. H. Santschi (2012), ^{234}Th in different size classes of sediment trap collected particles from the Northwestern Pacific Ocean, *Geochim. Cosmochim. Acta*, *91*, 60–74.

Hutchins, D. A., F.-X. Fu, Y. Zhang, M. E. Warner, Y. Feng, K. Portune, P. W. Bernhardt, and M. R. Mulholland (2007), CO_2 control of *Trichodesmium* N_2 fixation, photosynthesis, growth rates, and elemental ratios: Implications for past, present, and future ocean biogeochemistry, *Limnol. Oceanogr.*, *52*(4), 1293–1304, doi:10.4319/lo.2007.52.4.1293.

Jacquet, S. H. M., P. J. Lam, T. W. Trull, and F. Dehairs (2011), Carbon export production in the subantarctic zone and polar front zone south of Tasmania, *Deep Sea Res., Part II*, *58*(21–22), 2277–2292, doi:10.1016/j.dsr2.2011.05.035.

Karl, D., A. Michaels, B. Bergman, D. Capone, E. Carpenter, R. Letelier, F. Lipschultz, H. Paerl, D. Sigman, and L. Stal (2002), Dinitrogen fixation in the world's oceans, *Biogeochemistry*, *57*, 47–98.

Karl, D. M. (2002), Nutrient dynamics in the deep blue sea, *Trends Microbiol.*, *10*(9), 410–418.

Keeling, R. F., A. Körtzinger, and N. Gruber (2010), Ocean deoxygenation in a warming world, *Annu. Rev. Mar. Sci.*, *2*, 199–229.

Kostadinov, T. S., D. A. Siegel, and S. Maritorena (2010), Global variability of phytoplankton functional types from space: Assessment via the particle size distribution, *Biogeosciences*, *7*(3), 3239–3257, doi:10.5194/bg-7-3239-2010.

Kostadinov, T. S., D. A. Siegel, S. Maritorena, and N. Guillocheau (2012), Optical assessment of particle size and composition in the Santa Barbara Channel, California, *Appl. Opt.*, *51*(16), 3171–3189.

Lalande, C., S. B. Moran, P. Wassmann, J. M. Grebmeier, and L. W. Cooper (2008), ^{234}Th-derived particulate organic carbon fluxes in the northern Barents Sea with comparison to drifting sediment trap fluxes, *J. Mar. Syst.*, *73*(1), 103–113.

Lam, P. J., and J. K. B. Bishop (2007), High biomass, low export regimes in the Southern Ocean, *Deep Sea Res., Part II*, *54*(5–7), 601–638, doi:10.1016/j.dsr2.2007.01.013.

Lam, P. J., S. C. Doney, and J. K. B. Bishop (2011), The dynamic ocean biological pump: Insights from a global compilation of particulate organic carbon, $CaCO_3$, and opal concentration profiles from the mesopelagic, *Global Biogeochem. Cycles*, *25*, GB3009, doi:, doi:10.1029/2010GB003868.

Landry, M. R., K. E. Selph, A. G. Taylor, M. Décima, W. M. Balch, and R. R. Bidigare (2011), Phytoplankton growth, grazing and production balances in the HNLC equatorial Pacific, *Deep Sea Res., Part II*, *58*(3–4), 524–535, doi:10.1016/j.dsr2.2010.08.011.

Le Moigne, F. A. C., S. A. Henson, R. J. Sanders, and E. Madsen (2013), Global database of surface ocean particulate organic carbon export fluxes diagnosed from the ^{234}Th technique, *Earth Syst. Sci. Data Discuss.*, *6*(1), 163–187.

Lepore, K., S. B. Moran, A. B. Burd, G. A. Jackson, J. N. Smith, R. P. Kelly, H. Kaberi, S. Stavrakakis, and G. Assimakopoulou (2009), Sediment trap and in-situ pump size-fractionated POC/^{234}Th ratios in the Mediterranean Sea and Northwest Atlantic: Implications for POC export, *Deep Sea Res., Part I*, *56*(4), 599–613.

Liu, K.-K., and I. R. Kaplan (1989), The eastern tropical Pacific as a source of ^{15}N-enriched nitrate in seawater off southern California, *Limnol. Oceanogr.*, *34*(5), 820–830.

Lomas, M. W., and S. B. Moran (2011), Evidence for aggregation and export of cyanobacteria and nano-eukaryotes from the Sargasso Sea euphotic zone, *Biogeosciences*, *8*(1), 203–216.

Luo, Y. (2013), Applications of U-decay series isotopes to studying the meridional overturning circulation and particle dynamics in the ocean, PhD thesis, Fac. of Graduate Studies-Oceanography, Univ. of British Columbia, Vancouver, Canada.

Lynn, R. J., and J. J. Simpson (1987), The California Current System: The seasonal variability of its physical characteristics, *J. Geophys. Res.*, *92*(C12), 12,947–12,966, doi:10.1029/JC092iC12p12947.

Lyons, G., C. R. Benitez-Nelson, and R. C. Thunell (2011), Phosphorus composition of sinking particles in the Guaymas Basin, Gulf of California, *Limnol. Oceanogr.*, *56*(3), 1093–1105.

Maiti, K., C. R. Benitez-Nelson, and K. O. Buesseler (2010), Insights into particle formation and remineralization using the short-lived radionuclide, Thorium-234, *Geophys. Res. Lett.*, *37*, L15608, doi:10.1029/2010GL044063.

Maiti, K., M. A. Charette, K. O. Buesseler, and M. Kahru (2013), An inverse relationship between production and export efficiency in the Southern Ocean, *Geophys. Res. Lett.*, *40*, 1557–1561, doi:10.1002/grl.50219.

Martin, J. H., G. A. Knauer, D. M. Karl, and W. W. Broenkow (1987), VERTEX: Carbon cycling in the northeast Pacific, *Deep Sea Res., Part A*, *34*(2), 267–285, doi:10.1016/0198-0149(87)90086-0.

Mayor, D. J., R. Sanders, S. L. C. Giering, and T. R. Anderson (2014), Microbial gardening in the ocean's twilight zone: Detritivorous metazoans benefit from fragmenting, rather than ingesting, sinking detritus, *BioEssays*, *36*(12), 1132–1137, doi:10.1002/bies.201400100.

Michaels, A. F., and M. W. Silver (1988), Primary production, sinking fluxes and the microbial food web, *Deep Sea Res., Part A*, *35*(4), 473–490.

Moran, S. B., S. E. Weinstein, H. N. Edmonds, J. N. Smith, R. P. Kelly, M. E. Q. Pilson, and W. G. Harrison (2003), Does ^{234}Th/^{238}U disequilibrium provide an accurate record of the export flux of particulate organic carbon from the upper ocean?, *Limnol. Oceanogr.*, *48*(3), 1018–1029.

Morán, X. A. G., Á. López-Urrutia, A. Calvo-Díaz, and W. K. W. Li (2010), Increasing importance of small phytoplankton in a warmer ocean, *Global Chang. Biol.*, *16*(3), 1137–1144.

Murray, J. W., J. Young, J. Newton, J. Dunne, T. Chapin, B. Paul, and J. J. McCarthy (1996), Export flux of particulate organic carbon from the central equatorial Pacific determined using a combined drifting trap-^{234}Th approach, *Deep Sea Res., Part II*, *43*(4–6), 1095–1132.

Passow, U. (2002), Transparent exopolymer particles (TEP) in aquatic environments, *Prog. Oceanogr.*, *55*(3–4), 287–333, doi:10.1016/S0079-6611(02)00138-6.

Pates, J. M., and G. K. P. Muir (2007), U-salinity relationships in the Mediterranean: Implications for ^{234}Th:^{238}U particle flux studies, *Mar. Chem.*, *106*(3–4), 530–545.

Paulmier, A., and D. Ruiz-Pino (2009), Oxygen minimum zones (OMZs) in the modern ocean, *Prog. Oceanogr.*, *80*(3), 113–128.

Peterson, B. J., and B. Fry (1987), Stable isotopes in ecosystem studies, *Annu. Rev. Ecol. Syst.*, *293–320*.

Pike, S. M., K. O. Buesseler, J. Andrews, and N. Savoye (2005), Quantification of Th-234 recovery in small volume seawater samples by inductively coupled plasma-mass spectrometry, *J. Radioanal. Nucl. Chem.*, *263*, 355–360.

Planchon, F., A.-J. Cavagna, D. Cardinal, L. André, and F. Dehairs (2013), Late summer particulate organic carbon export and twilight zone remineralisation in the Atlantic sector of the Southern Ocean, *Biogeosciences*, *10*(2), 803–820, doi:10.5194/bg-10-803-2013.

Prahl, F. G., B. N. Popp, D. M. Karl, and M. A. Sparrow (2005), Ecology and biogeochemistry of alkenone production at Station {ALOHA}, *Deep Sea Res., Part I*, *52*(5), 699–719, doi:10.1016/j.dsr.2004.12.001.

Richardson, A. J., and D. S. Schoeman (2004), Climate impact on plankton ecosystems in the Northeast Atlantic, *Science*, *305*(5690), 1609–1612, doi:10.1126/science.1100958.

Richardson, T. L., and G. A. Jackson (2007), Small phytoplankton and carbon export from the surface ocean, *Science*, *315*(5813), 838–840.

Roden, G. I. (1958), Oceanographic and meteorological aspects of the Gulf of California, *J. Mar. Res.*, *18*, 10–35.

Rutgers van der Loeff, M. M., K. Buesseler, U. Bathmann, I. Hense, and J. Andrews (2002), Comparison of carbon and opal export rates between summer and spring bloom periods in the region of the Antarctic Polar Front, SE Atlantic, *Deep Sea Res., Part II*, *49*(18), 3849–3869.

Santamaría-del-Angel, E., S. Alvarez-Borrego, and F. E. Müller-Karger (1994), Gulf of California biogeographic regions based on coastal zone color scanner imagery, *J. Geophys. Res.*, *99*(C4), 7411–7421, doi:10.1029/93JC02154.

Santschi, P. H., C. C. Hung, G. Schultz, N. Alvarado-Quiroz, L. Guo, J. Pinckney, and I. Walsh (2003), Control of acid polysaccharide production and ^{234}Th and POC export fluxes by marine organisms, *Geophys. Res. Lett.*, *30*(2), 1044, doi:10.1029/2002GL016046.

Scharek, R., L. M. Tupas, and D. M. Karl (1999), Diatom fluxes to the deep sea in the oligotrophic North Pacific gyre at Station ALOHA, *Mar. Ecol. Prog. Ser.*, *182*, 55–67.

Schmidt, S., V. Andersen, S. Belviso, and J.-C. Marty (2002), Strong seasonality in particle dynamics of north-western Mediterranean surface waters as revealed by ^{234}Th/^{238}U, *Deep Sea Res., Part I*, *49*(8), 1507–1518, doi:10.1016/S0967-0637(02)00039-0.

Smoak, J. M., W. S. Moore, R. C. Thunell, and T. J. Shaw (1999), Comparison of ^{234}Th, ^{228}Th, and ^{210}Pb fluxes with fluxes of major sediment components in the Guaymas Basin, Gulf of California, *Mar. Chem.*, *65*(3), 177–194.

Speicher, E. A., S. B. Moran, A. B. Burd, R. Delfanti, H. Kaberi, R. P. Kelly, C. Papucci, J. N. Smith, S. Stavrakakis, and L. Torricelli (2006), Particulate organic carbon export fluxes and size-fractionated POC/^{234}Th ratios in the Ligurian, Tyrrhenian and Aegean Seas, *Deep Sea Res., Part I*, *53*(11), 1810–1830.

Stewart, G., J. K. Cochran, J. C. Miquel, P. Masqué, J. Szlosek, A. M. Rodriguez y Baena, S. W. Fowler, B. Gasser, and D. J. Hirschberg (2007), Comparing POC export from ^{234}Th/^{238}U and ^{210}Po/^{210}Pb disequilibria with estimates from sediment traps in the northwest Mediterranean, *Deep Sea Res., Part I*, *54*(9), 1549–1570.

Stewart, G., S. B. Moran, M. W. Lomas, and R. P. Kelly (2011), Direct comparison of ^{210}Po, ^{234}Th and POC particle-size distributions and export fluxes at the Bermuda Atlantic Time-series Study (BATS) site, *J. Environ. Radioact.*, *102*(5), 479–489.

Stewart, G. M., S. Bradley Moran, and M. W. Lomas (2010), Seasonal POC fluxes at BATS estimated from ^{210}Po deficits, *Deep Sea Res., Part I*, *57*(1), 113–124.

Szlosek, J., J. K. Cochran, J. C. Miquel, P. Masqué, R. A. Armstrong, S. W. Fowler, B. Gasser, and D. J. Hirschberg (2009), Particulate organic carbon–^{234}Th relationships in particles separated by settling velocity in the northwest Mediterranean Sea, *Deep Sea Res., Part II*, *56*(18), 1519–1532.

Taylor, G. T., F. E. Muller-Karger, R. C. Thunell, M. I. Scranton, Y. Astor, R. Varela, L. T. Ghinaglia, L. Lorenzoni, K. A. Fanning, and S. Hameed (2012), Ecosystem responses in the southern Caribbean Sea to global climate change, *Proc. Natl. Acad. Sci. U.S.A.*, *109*(47), 19,315–19,320.

Thomalla, S. J., R. Turnewitsch, M. Lucas, and A. Poulton (2006), Particulate organic carbon export from the North and South Atlantic gyres: The ^{234}Th/^{238}U disequilibrium approach, *Deep Sea Res., Part II*, *53*(14–16), 1629–1648.

Thunell, R., C. Pride, P. Ziveri, F. Muller-Karger, C. Sancetta, and D. Murray (1996), Plankton response to physical forcing in the Gulf of California, *J. Plankton Res.*, *18*(11), 2017–2026.

Thunell, R. C. (1998), Seasonal and annual variability in particle fluxes in the Gulf of California: A response to climate forcing, *Deep Sea Res., Part I*, *45*(12), 2059–2083.

Trent, J. D., A. L. Shanks, and M. W. Silver (1978), In situ and laboratory measurements on macroscopic aggregates in Monterey Bay, California, *Limnol. Oceanogr.*, *23*(4), 626–635.

Twardowski, M. S., J. M. Sullivan, P. L. Donaghay, and J. R. V. Zaneveld (1999), Microscale quantification of the absorption by dissolved and particulate material in coastal waters with an ac-9, *J. Atmos. Oceanic Technol.*, *16*(6), 691–707.

Van Mooy, B. A. S., R. G. Keil, and A. H. Devol (2002), Impact of suboxia on sinking particulate organic carbon: Enhanced carbon flux and preferential degradation of amino acids via denitrification, *Geochim. Cosmochim. Acta*, *66*(3), 457–465.

Verdugo, P., A. L. Alldredge, F. Azam, D. L. Kirchman, U. Passow, and P. H. Santschi (2004), The oceanic gel phase: A bridge in the DOM-POM continuum, *Mar. Chem.*, *92*(1–4), 67–85.

Wakeham, S. G., and E. A. Canuel (1988), Organic geochemistry of particulate matter in the eastern tropical North Pacific Ocean: Implications for particle dynamics, *J. Mar. Res.*, *46*(1), 183–213.

White, A. E., F. G. Prahl, R. M. Letelier, and B. N. Popp (2007), Summer surface waters in the Gulf of California: Prime habitat for biological N_2 fixation, *Global Biogeochem. Cycles*, *21*, GB2017, doi:10.1029/2006GB002779.

White, A. E., R. A. Foster, C. R. Benitez-Nelson, P. Masqué, E. Verdeny, B. N. Popp, K. E. Arthur, and F. G. Prahl (2013), Nitrogen fixation in the Gulf of California and the Eastern Tropical North Pacific, *Prog. Oceanogr.*, *109*, 1–17.

Xu, C., P. H. Santschi, C. C. Hung, S. Zhang, K. A. Schwehr, K. A. Roberts, L. Guo, G. C. Gong, A. Quigg, and R. A. Long (2011), Controls of ^{234}Th removal from the oligotrophic ocean by polyuronic acids and modification by microbial activity, *Mar. Chem.*, *123*(1–4), 111–126.

Ziveri, P., and R. C. Thunell (2000), Coccolithophore export production in Guaymas Basin, Gulf of California: Response to climate forcing, *Deep Sea Res., Part II*, *47*(9–11), 2073–2100.